INTENSE LASER-GAS INTERACTIONS IN HOLLOW-CORE PHOTONIC BAND-GAP FIBERS

A Dissertation

Presented to the Faculty of the Graduate School

of Cornell University

in Partial Fulfillment of the Requirements for the Degree of

Doctor of Philosophy

by

Christopher James Hensley

February 2010

INTENSE LASER-GAS INTERACTIONS IN HOLLOW-CORE PHOTONIC BAND-GAP FIBERS

Christopher James Hensley, Ph.D.

Cornell University 2010

This dissertation presents an experimental investigation of intense laser field propagation in hollow-core photonic band-gap fibers (HC-PBGF). The primary aim of this work has been the production of coherent extreme ultraviolet radiation by high-harmonic generation in a gas-filled fiber. The geometric properties of HC-PBGFs have the potential for a dramatic reduction of the pulse energy previously required while the guiding principles should permit enhanced conversion by phase-matching the fundamental and harmonic waves. In this effort we also studied the glass contribution to the nonlinearity of these unique fibers showing the significant change that can occur by nanometer scale deviations in the core structure. We also, by careful mode matching to the fundamental fiber mode, demonstrated record-low coupling losses which allowed peak intensity transmission nearly an order of magnitude larger than previously observed. To avoid nonlinear effects while coupling into the high-harmonic generating fiber and absorption effects when coupling out xenon was introduced by a microchannel drilled through the side of the fiber with ultrafast-laser pulses. Though we were unable to observe high harmonic generation significant progress was made toward this goal including assembly and optimization of the vacuum chamber, construction of a gas-to-fiber delivery system and characterization of our detector by generating third harmonic in a continuous jet of xenon.

BIOGRAPHICAL SKETCH

Christopher was born in November of 1980 five years to the day from the wreck of the Edmund Fitzgerald in Lake Superior. He was raised with love by his parents and two older sisters, Jill and Cory in White Bear Lake, Minnesota. His early interest in taking things apart and putting them back together eventually led him to science and a desire to figure out how things work. After receiving degrees in Physics and Mathematics at the University of St. Thomas in 2003 he took his studies on the road to Ithaca, New York and Cornell University. After six years of graduate research investigating intense-field interactions with matter he is carrying his skills back to Minnesota to explore nonlinear optical interactions with molecular states. He is still trying to figure out how things work.

"The universe is a big place, perhaps the biggest."

-Kurt Vonnegut

ACKNOWLEDGEMENTS

To begin, I would like to thank my advisor Professor Alexander Gaeta for the opportunity to work in his lab. Alex has been a consistent source of motivation and a calm voice of reason throughout my time at Cornell.

My regards to Chris Schaffer, who was instrumental in the femtsecond-laser machining work presented in this dissertation, his kindness and generosity with his time is probably why he is up until three in the morning every night. A thanks to our collaborators at Corning, who supplied us with hollow-core photonic fiber and in particular Karl Koch with whom I shared many insightful discussions.

Also, all the current and past members of the Gaeta Group with whom I had the pleasure to work along side. A special debt to Dimitre Ouzounov who showed me the ins and outs of hollow-core fibers, Jay Sharping who taught me how to cleave and splice fiber optics like a professional, my ultrafast-laser machining colleague Daniel Broaddus and Mark Foster, our information technology expert, who showed me how to do everything else.

I would like to acknowledge Lawrence Livermore National Laboratories for their financial support through the National Physical Science Consortium.

Lastly, I owe the biggest thanks and appreciation to my wonderful wife, Kirsten. She has been my greatest supporter through these years and I can not imagine having done this without her.

TABLE OF CONTENTS

LIST OF TABLES

LIST OF FIGURES

CHAPTER 1

INTRODUCTION

Frequency conversion is a branch of nonlinear optics concerning the production of new optical wavelengths by nonlinear methods. In parametric processes such as second harmonic, sum and difference frequency generation a propagating optical field induces a polarization which creates new frequencies [1]. The first demonstration of this was observed shortly after the development of the laser when a millisecond-pulsed ruby laser was focused into a piece of crystalline quartz to create second harmonic blue light [2]. A more dramatic demonstration of nonlinear frequency conversion was found many years later when an amplified laser system was focused into a gas jet to produce higher order harmonics of the fundamental [3]. Initially producing radiation into the vacuum ultraviolet, high harmonic generation has been used to create radiation up to the 221st harmonic [4]. This coherent short wavelength radiation carries the potential to produce sharper lithographic features [5, 6] for next generation EUV lithography as well as improved temporal resolution with high harmonic generation opening a route for attosecond pulse generation [7, 8]. Previous work has demonstrated the ability to phase match this process in hollow capillary tubes to increase the conversion efficiency. By shrinking these dimensions further in a hollow-core photonic band-gap fiber (HC-PBGF) one anticipates efficient conversion at a lower pulse energy allowing for high-repetition rate sources for coherent extreme ultraviolet radiation. This chapter presents an overview of hollow-core photonic band-gap fibers, a brief discussion of intense-field nonlinear optics and high harmonic generation and the theory and capabilites of ultrafast-laser micromachining. The rest of the dissertation is organized as follows.

Chapter 2 discusses studies of the glass contribution to the nonlinearity of HC-PBGFs. Although the majority of the fundamental mode of these fibers resides within the air-core region there is a fraction of light that interacts with the glass [9]. With the significantly larger nonlinear coefficient of glass compared to air this can create an almost equivalent contribution to the total fiber nonlinearity [10]. By evacuating the fiber we eliminate the air contribution and investigate how small structural changes impact the fraction of the propagating mode that resides in the glass.

Chapter 3 presents investigations into the maximum coupling and damage threshold of these fibers in the femtosecond-pulse regime. The required intensities for observing high harmonic generation are beyond previously observed peak transmitted intensities through these fibers [11]. Here we present a careful study demonstrating a significant decrease in the coupling losses and a corresponding increase in the delivered intensity.

Chapter 4 describes microfabrication of a channel through the side of a HC-PBGF using tightly focused femtosecond-laser pulses. This access port allows for direct introduction of gas into the fiber core and variable-pressure filling of all-fiber gas cells. A recently developed technique, ultrafast-laser micromachining is a rapidly growing area and has the potential for numerous applications in post-processing of HC-PBGF.

In chapter 5 we discuss progress in attaining our goal of observing high-harmonic generation in a HC-PBGF. By a combination of efforts from the preceding chapters we create the ideal conditions for observing high harmonics and discuss limiting factors to this success. Phase matching of this process in HC-PBGFs and a potential mechanism for quasi-phase matching inside these

gas-filled fibers is also discussed.

Chapter 6 presents concluding remarks and future work to explore in the area of high-harmonic generation inside HC-PBGF and ultrafast-laser machining inside these unique fibers.

1.1 Hollow-core photonic band-gap fibers

In the early 1970s the efficient transmission of communication signals through gas or vacuum was first proposed [12]. At the time this meant waveguiding with glass capillaries which supported multiple modes and had very high losses. Hollow-core photonic band-gap fibers are a unique class of photonic crystal fiber that guide single-mode light with low loss in air [13]. The mechanism for this guidance is multiple coherent scattering from a two-dimensional microstructure surrounding the core. Developed in the late 1990s, HC-PBGFs were originally put forth as a means of reducing loss in data and communication lines[14]. Simulated models show extremely low loss for wavelengths confined by the band-gap of these fibers with theoretical attenuation as low as 0.2 dB/km [15]. However, the complicated, nanometer-scale structure of HC-PBGFs makes fabrication of these fibers challenging, and the attenuation in early samples was approximately 1000 dB/km [16, 17]. Since the reduction of transmission losses in HC-PBGFs [15, 18], these fibers have found use in areas such as wavelength conversion, pulse compression and delivery, gas sensing, and resonant optical interactions [11, 19, 20, 21, 22, 23, 24, 25].

Theoretical descriptions of guiding in HC-PBGFs follow from work done by Yeh and Yariv in the 1970s [26, 27]. Using an analogy with electrons in a solid

they describe periodically layered material in terms of Bloch waves and band structures. By the late 1980s this formalism was extended to show frustrated transmission of certain wavelengths in a defect region [28, 29]. Building upon these studies, in the 1990s, various models of two-dimensional photonic band-gap structures for light guidance were proposed [30, 31, 32] eventually leading to a physical demonstration of single-mode guidance in an air core[13].

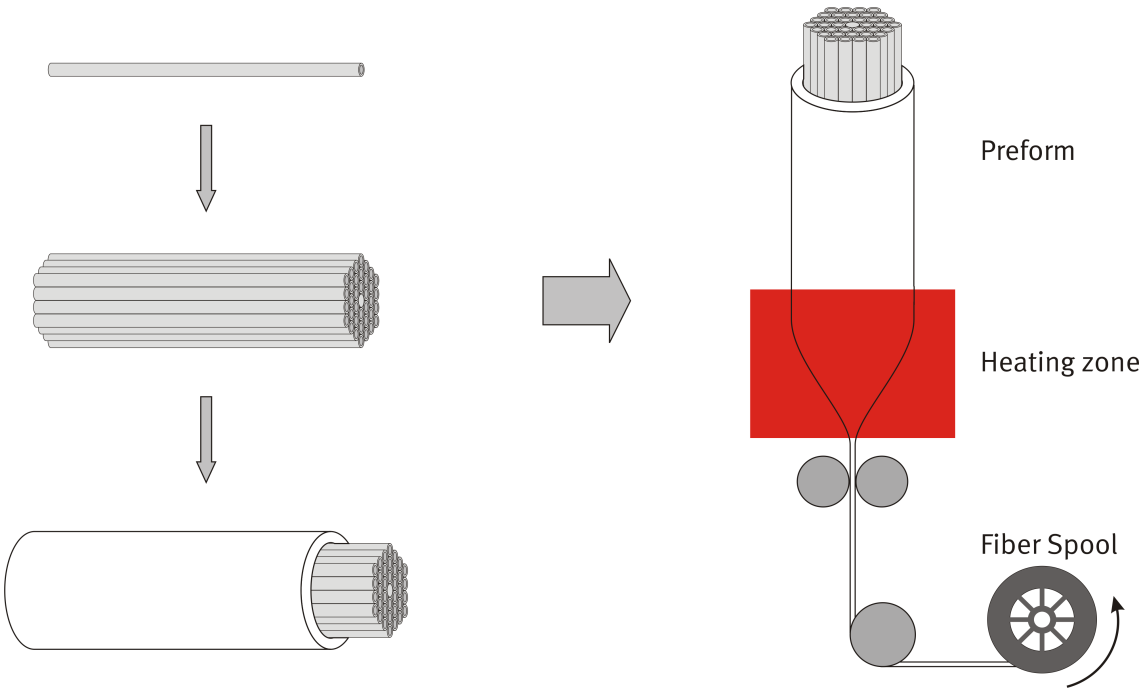

Figure 1.1: An illustration of the process for hollow-core photonic band-gap fiber fabrication. The outer diameters of these initial capillaries are ~1 mm. *Image courtesy of Richard Ramsey, NKT Photonics.*

Fabrication of HC-PBGFs follow a method similar to that used for standard step-index telecommunication fiber [33]. To begin, meter-length circular capillaries are stacked into the desired shape with seven (or 19) capillaries removed to form the defect core. These are then wrapped in wire and inserted into a jacketing tube to produce a preform. This preform is then drawn down to fiber

inside a furnace run at 1800-2000° C, see Figure 1.1. By careful manipulation of gas flow precision control of the microstructure pitch and thickness is possible, although several iterations are typically required in drawing out a new fiber design. Typical to all optical fiber the large extension ratio from preform to fiber tends to smooth out distortions in the initial stack of capillaries and results in extraordinary uniformity along the length of the fiber. However, roughness does remain at the air-glass interfaces and has been used to account for the attenuation seen in HC-PBGFs [15].

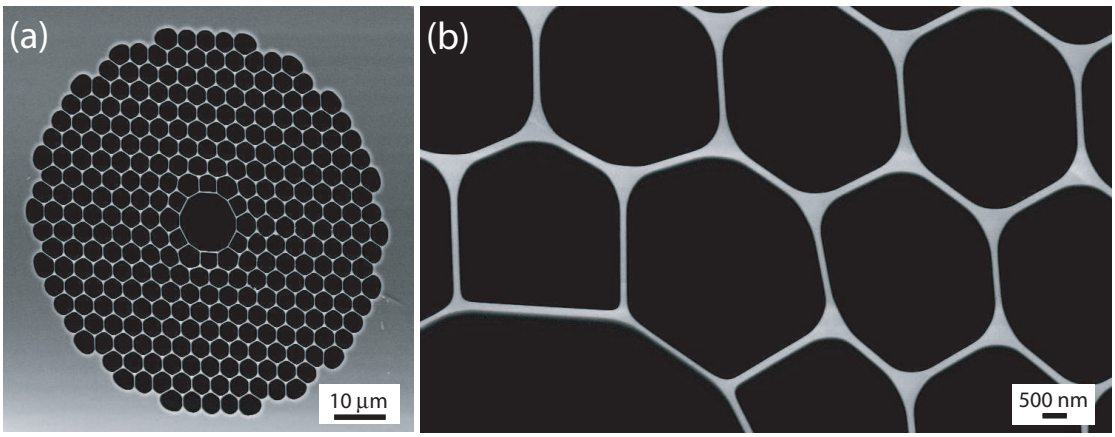

Figure 1.2: (a) Scanning electron micrograph image of hollow-core photonic band-gap fiber (b) the core walls and lattice structure of these fibers are less than 100 nm wide.

To find applications in long-haul telecommunications, HC-PBGFs will need to exhibit loss that is comparable to or less than that of step-index silica fibers (0.15 dB/km). However, there are other applications that require delivery of high-energy pulses, for which HC-PBGFs have already demonstrated significant advantages over glass-core fibers [34, 35]. Also, by matching the dispersion and nonlinearity of these fibers high-power optical solitons have been generated in the femtosecond regime [11, 10] and used for temporal compression [20]. The

unique geometry of these fibers allows for an unprecedented tight confinement in air-guided transmission allowing for intense peak fields with only modest pulse energies. A generic feature of HC-PBGF's is that the group-velocity dispersion (GVD) is anomalous over most of the transmission window [11], which makes them suitable for dispersive elements in high-power fiber lasers and amplifiers [36, 37, 38, 39, 40]

The long interaction lengths afforded in these fibers make them ideal for low-level light-matter studies as well. Resonant optical interactions and electromagnetic induced transparency have been demonstrated with extremely low thresholds in HC-PBGF filled with acetylene and rubidium gas [23, 25]. Recent work in rubidium-filled HC-PBGFs has demonstrated four-wave mixing gain [41] and all-optical switching with very low-light levels [42]. Interest in HC-PBGFs continues to grow as increasing numbers of applications are discovered.

1.2 Intense-Field Nonlinear Optics

Nonlinear optical phenomena is generally described through a Taylor series expansion of the dielectric polarization in the applied electric field [1] given by

$$P(t) = \chi^{(1)}E(t) + \chi^{(2)}E(t)^2 + \chi^{(3)}E(t)^3 + \cdots. \tag{1.1}$$

For non-resonant parametric processes such as second-harmonic generation, third-harmonic generation and four-wave mixing this perturbation theory gives an adequate description. However, as the applied laser approaches the atomic field strength intensity of

$$I_{at} = \frac{c}{8\pi} E_{at}^2 = \frac{e^2 c}{8\pi a_o^4} = 4 \times 10^{16} W/cm^2 \tag{1.2}$$

this series ceases to converge. Under this condition the influence of the laser field dominates electron motion which is described by the equation of motion

$$m\ddot{x} = -eEe^{-i\omega t} \tag{1.3}$$

which has the solution

$$x(t) = eE/m\omega^2. \tag{1.4}$$

With this one can then define the time-averaged kinetic energy associated with this motion, also termed the ponderomotive energy [43]

$$U_p = e^2 E_{peak}^2 / 4m\omega^2. \tag{1.5}$$

This energy related to the jitter of the electron about equilibrium can be substantial as the atomic field strength is approached by the incident laser intensity. At sufficient peak intensities (I $\cong 1 \times 10^{14}$), the associated ponderomotive energy (10.5 eV) becomes comparable to atomic ionization potentials (see Figure 1.3) producing conditions for observing unique phenomenon such as high harmonic generation.

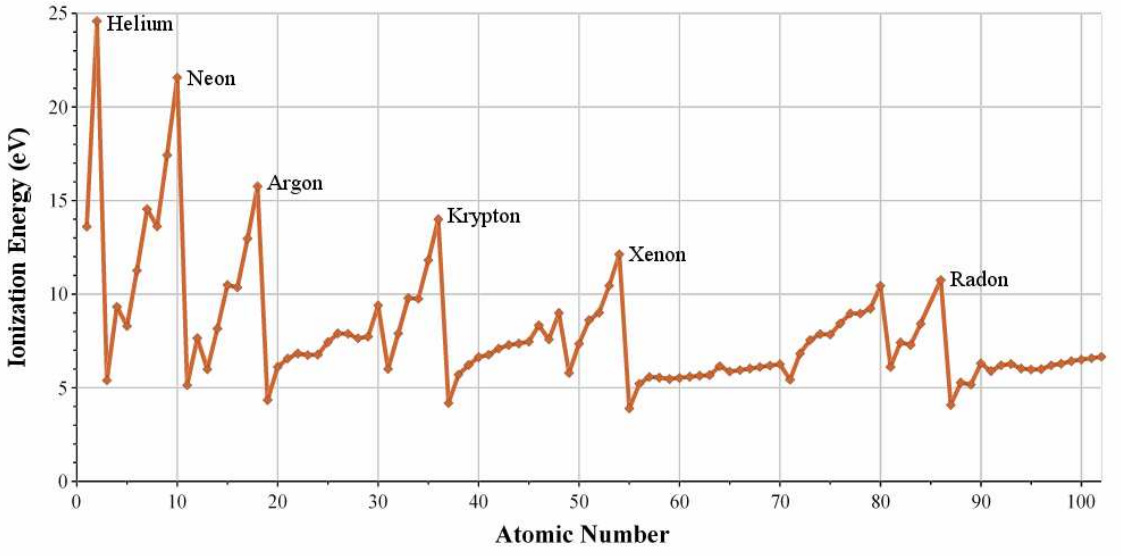

Figure 1.3: Ionization potentials plotted versus atomic number. The noble gases in which high harmonic generation is typically observed have the largest potentials. Data from reference [44].

High Harmonic Generation

Frequency conversion under strong-field conditions is an extraordinary event that can yield photons of a few hundred eV from an incident infrared laser. This process of high harmonic generation can be described semi-classically by a simple model proposed by Corkum [45]. This description imagines an intense linearly-polarized laser field incident on an atom causing ionization. This ionized electron is then driven, under the influence of the oscillatory optical field, away from the atom and then quickly accelerated back. With additional kinetic energy acquired from the laser field, the electron emits short-wavelength radiation upon recombination with the atom. In a collection of atoms these return collisions creates a pulse train separated by half the optical period of the fundamental. Taking the Fourier transform gives the generated spectrum in the form of odd harmonics of the incident field. As both the electron path and re-

combination are driven by the fundamental laser field, this process results in radiation that is both temporally and spatially coherent. Included in this model is the maximum harmonic n_{max} that can be produced as a function of the incident ponderomotive energy

$$E_{max} = n_{max}\hbar\omega = 3.17U_p + I_p. \tag{1.6}$$

where I_p is the negative ionization potential of the atom. Although a more complete theoretical description of this process including secondary electron effects as well as quantum mechanical description of the field has been produced , Corkum's model still adequately predicts the majority of high harmonic experiments.

The initial demonstration of high harmonic generation was done using a gas jet at a relatively low peak intensity of 3×10^{13} W/cm^2 [3]. In this work a 1064 nm Nd:YAG laser was converted to vacuum ultraviolet radiation as short as the 33rd harmonic with argon gas. Since then much work has been done to push to higher harmonics and more efficient conversion [46, 47, 48, 49]. Shorter ultrafast pulses give a convenient route to higher peak intensities and few-cycle pulse have been used to enhance conversion and extend radiation into the water window (2.3-4.4 nm) [50]. Another path for enhancing conversion is phase-matching of the process in hollow capillaries [51]. Since the fundamental and high harmonics are greatly separated in frequency, the ability to match phase velocities can be challenging and requires some novel techniques. With the large peak intensities required for this process, high harmonic generation is typically observed using low-repetition rate amplified lasers. In an effort to increase the total flux of harmonics generated, methods such as enhancement cavites [52, 53]

and resonant plasmon field enhancement [64] allowing for harmonic generation with repetition rates beyond 100 MHz.

1.3 Optical Breakdown

Much like the observation of second-harmonic generation the invention of the laser was quickly followed by the discovery of optical breakdown [55]. Optical breakdown, or optically-induced damage, occurs when an intense laser field generates a plasma in a gas or condensed material. In solid materials this critical electron density then transfers energy to the lattice in a catastrophic event resulting in permanent damage. This process differs from thermal breakdown in which linear absorption results in localized heating and cracking of the optical material. For transparent material, in which linear absorption does not occur, the mechanism for this plasma formation is nonlinear photoionization followed by avalanche ionization which creates an excess of excited electrons. The intensities required for this breakdown to occur are readily achieved by pulsed lasers and for ultrafast laser pulses the associated damage can be highly deterministic.

In a material with a band gap exceeding the energy of the incident photons there are two mechanisms by which electron excitation can result. The first is multiphoton excitation in which multiple photons combine to excite a valence electron into the conduction band. Multiphoton excitation is the dominant process for low intensity lasers or short wavelengths in which the band gap energy does not greatly exceed the incident photon energy. For adequately intense laser fields or long wavelengths the nonlinear excitation is described by quantum mechanical tunneling [56]. Under these conditions the Coulomb field

of the atom is suppressed by the incident laser field allowing electrons to tunnel ionize through the remaining potential. The transition between these two mechanism is defined by the Keldysh parameter

$$\gamma = \frac{\omega}{e}\sqrt{\frac{mcn\epsilon_o E_g}{I}}, \tag{1.7}$$

where n is the refractive index, E_g is the energy gap of the material and I is the intensity of the incident laser field. For $\gamma > 1.5$ multiphoton excitation is the main mechanism for electron promotion into the conduction and for $\gamma < 1.5$ tunneling dominates this process [57].

Upon promotion these conduction electrons combine linearly with incident photons until the electron's energy is more than twice that of the materials energy gap. At this point the highly energetic electron collides with a valence electron resulting in two electrons in the conduction band as shown in Figure 1.4. These two electrons can then again, through free-carrier absorption, be excited further until they collide with two more valence electrons and so on until a plasma is formed by this runaway process [58]. Once a critical plasma density is achieved energy can be efficiently transferred to the material which results in permanent damage.

Ultrafast-laser micromachining

Optical breakdown with ultrafast laser pulses follows the same excitation, absorption and energy transfer mechanism described above. However, by a combination of tight-focusing and very short laser pulses relatively little heating occurs in the surrounding lattice during ultrafast-laser machining [58]. That is,

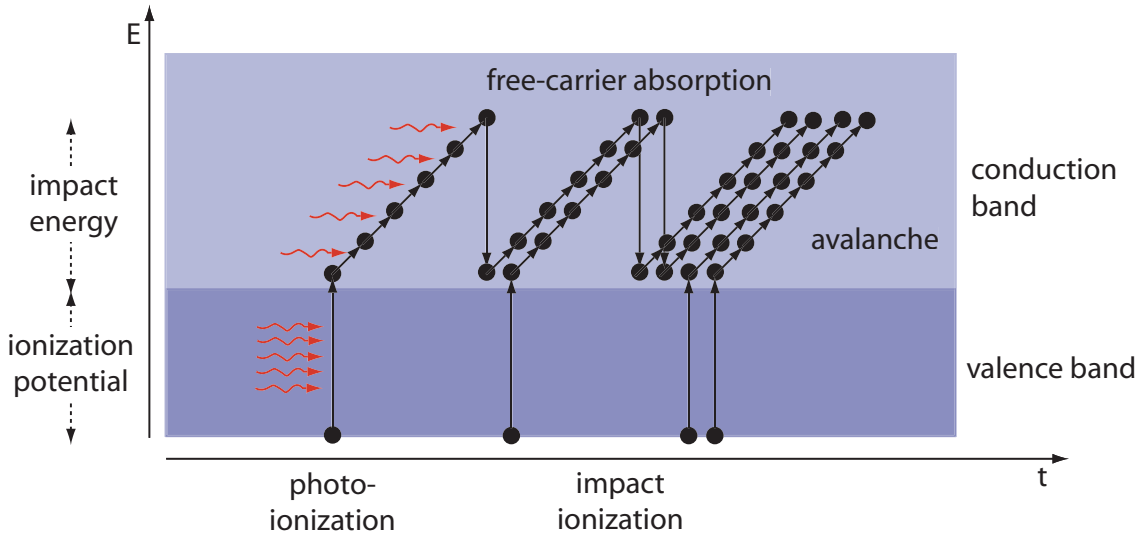

Figure 1.4: An illustration of the mechanism for plasma formation through photoionization, free-carrier absorption and impact ionization.

with rapid heating of conduction electrons, energy is transferred to the lattice faster than the thermal diffusion time. What results is a shock-like deposition of energy creating ablation of material at the surface (Figure 1.5) and permanent structural change in bulk. This efficient route to optical breakdown requires much lower pulse energies when compared to standard laser-machining techniques that use longer pulses and thereby significantly reduces collateral thermal effects.

The predictability of damage from ultrafast lasers has led to applications in fabrication under the term femtosecond-laser micromachining [59]. Deterministic breakdown occurs due to the mechanism for electron promotion by short pulse lasers. For avalanche excitation to occur seed electrons are required in the conduction band. In the case of longer laser pulses this requires defects within the structure. Ultrafast lasers are self seeding in that photoionization on the front edge of an incident pulse is adequate to excite valence electrons giving

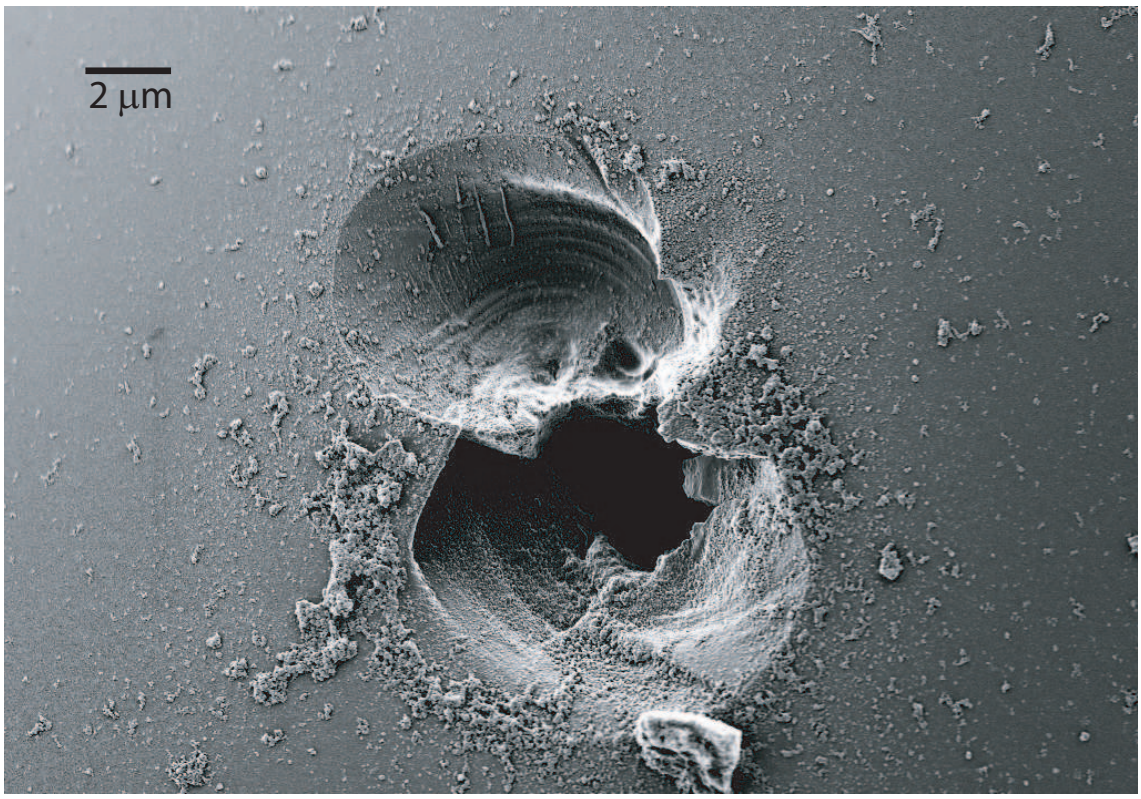

Figure 1.5: Surface of optical fiber that has been ablated with femtosecond laser pulses.

rise to the avalanche process [60].

By tightly focussing ultrafast laser pulses with a high numerical-aperture objective the intensities for optical breakdown are easily produced. This mechanism has been used to induce a change in refractive index for writing waveguides [61, 62] or to form vacancies [63] in fused silica. Recent work has demonstrated the ability to create sub-micrometer diameter capillaries in molded poly(dimethyl) siloxane [64], as well as in glass [65]. With material removal occurring only at the focus of the beam, the sample can be translated to make channels of a length limited only by debris removal [66]. This clearing of debris is facilitated by adding a fluid that wicks in the forming channel during fabri-

cation. For surface ablation debris redeposition has been avoided by purging with dry nitrogen [67].

The ability to remove material in three-dimensions and without thermal damage to the surrounding material has led to wide interest in femtosecond laser machining. With void formation as small as 100 nm in diameter in bulk [68] and surface structures as small as 30 nm [69], ablation with ultrafast lasers exhibits near nanofabrication capabilities. The capacity to induce breakdown at any point in a bulk transparent material should allow for niche applications such as the one presented in Chapter 4 of this dissertation.

REFERENCES

[1] R. W. Boyd, *Nonlinear Optics* (Academic, Boston, 1992).

[2] P. A. Franken, A. E. Hill, C. W. Peters and G. Weinreich, *Phys. Rev. Lett.* **7** (4), 118 (1961).

[3] M. Ferray, A. L'Huillier, X. F. Li, L. A. Lompre, G. Mainfray and C. Manus, *J. Phys. B: At. Mol. Opt. Phys.* **21** L31-L35 1988.

[4] Z. Chang, et al. *Phys. Rev. Lett.* **82**, 2006 (1999).

[5] H. H. Solak, D. He, W. Li, S. Singh-Gasson, F. Cerrina, B. H. Sohn, X. M. Yang and P. Nealey, *Appl. Phys. Lett.* **75**, 2328 (1999).

[6] P. W. Wachulak, M. G. Capeluto, M. C. Marconi, C. S. Menoni and J. J. Rocca, *Opt. Express* **15**, 3465-3469 (2007).

[7] P. M. Paul, E. S. Tomas, P. Breger, G. Mullot, F. Augé, P. Balcou, H. G. Muller and P. Agostini, *Science* **292**, 1689 (2001).

[8] P. Antoine, A. L'Huillier and M. Lewenstein, *Phys. Rev. Lett.* **77**, 1234-1237 (1996).

[9] C. J. Hensley, D. G. Ouzounov, A. L. Gaeta, N. Venkataraman, M. T. Gallagher and K. W. Koch, *Opt. Express* **15**, 35073512 (2007).

[10] F. Luan, J. C. Knight, P. St. J. Russell, S. Campbell, D. Xiao, D. T. Reid, B. J. Mangan, D. P. Williams and P. J. Roberts, *Opt. Express* **12**, 835-840 (2004).

[11] D. G. Ouzounov, F. R. Ahmad, D. Muller, N. Venkataraman, M. T. Gallagher, M. G. Thomas, J. Silcox, K. W. Koch, and A. L. Gaeta, *Science* **301**, 1702-1704 (2003).

[12] D. Gloge, *Proc. IEEE* **58**, 1513-1522 (1970).

[13] R. F. Cregan, B. J. Mangan, J. C. Knight, T. A. Birks, P. St. J. Russell, P. J. Roberts, and D. A. Allan, *Science* **285**, 1537-1539 (1999).

[14] P. Russell, *Science* **299**, 358362 (2003).

[15] P. Roberts, F. Couny, H. Sabert, B. Mangan, D. Williams, L. Farr, M. Mason, A. Tomlinson, T. Birks, J. Knight, and P. St. J. Russell, *Opt. Express* **13**, 236-244 (2005).

[16] D. C. Allan, J. A. West, J. C. Fajardo, M. T. Gallagher, K. W. Koch, and N. F. Borrelli, in *Photonic crystals and Light Localization in the 21st Century*, C. M. Soukoulis, ed. (Kluwer Academic, Dordecht, Netherlands, 2001) pp. 305-320.

[17] J. A. West, N. Venkataraman, C. M. Smith, and M. T. Gallagher, in *Proceedings of European Conference on Optical Communication* (IEEE, 2001) pp. 582-585.

[18] C. M. Smith, N. Venkataraman, M. T. Gallagher, D. Muller, J. A. West, N. F. Borrelli, D. C. Allan, and K. W. Koch, *Nature* **424**, 657-659 (2003).

[19] F. Benabid, J. C. Knight, G. Antonopoulos, and P. St. J. Russell, *Science* **298**, 399-402 (2002).

[20] D. G. Ouzounov, C. J. Hensley, A. L. Gaeta, N. Venkateraman, M. T. Gallagher, and K. W. Koch, *Opt. Express* **13**, 6153-6159 (2005).

[21] T. Ritari, J. Tuominen, H. Ludvigsen, J. Petersen, T. Sørensen, T. Hansen, and H. Simonsen, *Opt. Express* **12**, 4080-4087 (2004).

[22] J. Henningsen, J. Hald, and J. C. Peterson, *Opt. Express* **13**, 10475-10482 (2005).

[23] S. Ghosh, J. E. Sharping, D. G. Ouzounov, and A. L. Gaeta, *Phys. Rev. Lett.* **94**, 093902 (2005).

[24] F. Benabid, P. Light, F. Couny, and P. Russell, *Opt. Express* **13**, 5694-5703 (2005).

[25] S. Ghosh, A. R. Bhagwat, C. K. Renshaw, S. Goh, A. L. Gaeta, and B. J. Kirby, *Phys. Rev. Lett.* **97**, 023603 (2006).

[26] P. Yeh and A. Yariv, *Opt. Commun.* **19**, 427430 (1976).

[27] P. Yeh, A. Yariv and C.-S. Hong, *J. Opt. Soc. Am.* **67**, 42338 (1977).

[28] E. Yablonovitch, *Phys. Rev. Lett.* **58**, 20592062 (1987).

[29] S. John, *Phys. Rev. Lett.* **58**, 24862489 (1987).

[30] P. R. Villeneuve and M. Piché, *Phys. Rev. B* **46**, 49694972 (1992).

[31] A. A. Maradudin and A. R. McGurn, *J. Mod. Opt.* **41**, 275284 (1994).

[32] T. A. Birks, P. J. Roberts, P. St. J. Russell, D. M. Atkin and T. J. Shepherd, *Electron. Lett.* **31**, 19411943 (1995).

[33] P. St. J. Russell, *J. Lightw. Technol.* **24**, 47294749 (2006).

[34] G. Humbert, J. C. Knight, G. Bouwmans, P. St. J. Russell, D. P. Williams, P. J. Roberts, B. J. Mangan, *Opt. Express* **12**, 1477-1484 (2004).

[35] J. D. Shephard, J. D. C. Jones, D. P. Hand, G. Bouwmans, J. C. Knight, P. St. J. Russell, and B. J. Mangan, *Opt. Express* **12**, 717-723 (2004).

[36] J. Limpert, T. Schreiber, S. Nolte, H. Zellmer and A. Tünnermann, *Opt. Express* **11**, 3332-3337 (2003).

[37] H. Lim and F. W. Wise, *Opt. Express* **12**, 2231-2235 (2004).

[38] C. de Matos, J. Taylor, T. Hansen, K. Hansen, and J. Broeng, *Opt. Express* **11**, 2832-2837 (2003).

[39] M. Rusu and O. G. Okhotnikov, *Appl. Phys. Lett.* **89**, 091118 (2006).

[40] C. K. Nielsen, K. G. Jespersen, and S. R. Keiding, *Opt. Express* **14**, 6063-6068 (2006).

[41] P. S. Londero, V. Venkataraman, A. R. Bhagwat, A. D. Slepkov, and A. L. Gaeta, *Phys. Rev. Lett.* **103**, 043602 (2009).

[42] M. Bajcsy, S. Hofferberth, V. Balic, T. Peyronel, M. Hafezi, A. S. Zibrov, V. Vuletic and M. D. Lukin, *Phys. Rev. Lett.* **102**, 203902 (2009).

[43] T. W. B. Kibble, *Phys. Rev Lett.* **16**, 1054 (1966).

[44] W. C. Martin, W. L. Wiese, *Atomic, Molecular, and Optical Physics Handbook* (American Institute of Physics, 1996).

[45] P. B. Corkum, *Phys. Rev. Lett.* **71** 1994 (1993).

[46] J. J. Macklin, J. D. Kmetec, and C. L. Gordon III, 1993, *Phys. Rev. Lett.* **70**, 766 (1993).

[47] Y. Tamaki, J. Itatani, Y. Nagata, M. Obara and K. Midorikawa, *Phys. Rev. Lett.* **82**, 1422 - 1425 (1999).

[48] R. Bartels, S. Backus, E. Zeek, L. Misoguit, G. Vdovin, I. P. Christov, M. M. Murnane and H. C. Kapteyn, *Nature* **406**, 164-166 (2000).

[49] T. Brabec and F. Krausz, *Rev. Mod. Phys.* **72**, (2000).

[50] Ch. Spielmann, N. H. Burnett, S. Sartania, R. Koppitsch, M. Schnürer, C. Kan, M. Lenzner, P. Wobrauschek, and F. Krausz, *Science* **278**, 661664 (1997).

[51] C. G. Durfee, A. R. Rundquist, S. Backus, C. Herne, M. M. Murnane and H. C. Kapteyn, *Phys. Rev. Lett.* **62** 524 (1999).

[52] R. J. Jones, K. D. Moll, M. J. Thorpe and J. Ye, *Phys. Rev. Lett.* **94**, 193201 (2005).

[53] D. C. Yost, T. R. Schibli and J. Ye, *Opt. Lett.* **33**, 1099-1101 (2008).

[54] S. Kim, J. Jin, Y-I. Kim, Y-J. Park, Y. Kim and S. W. Kim, *Nature* **453**, 757-760 (2008).

[55] P. D. Maker, R. W. Terhune, and C. M. Savage, Quantum Electronics III, edited by P. Grivet and N. Bloembergen (Columbia University Press, New York, 1964), p. 1559.

[56] M. V. Ammosov, N. B. Delone, and V. P. Krainov, *Sov Phys. JETP* **64**, 1191 (1986).

[57] K. V. Keldysh, *Sov. Phys. JETP* **20**, 1307 (1965).

[58] B. C. Stuart, M. D. Feit, S. Herman, A. M. Rubenchik, B. W. Shore and M. D. Perry, *Phys. Rev. B* 53, 1749 (1996).

[59] R. R. Gattass and E. Mazur, *Nat. Photon.* **2**, 219-225 (2008).

[60] D. Du, X. Liu, G. Korn, J. Squier, and G. Mourou, *Appl. Phys. Lett.* **64**, 3071-3073 (1994).

[61] K. M. Davis, K. Miura, N. Sugimoto, and K. Hirao, *Opt. Lett.* **21**, 1729-1731 (1996).

[62] D. Homoelle, S. Wielandy, N. Borrelli, C. Smith, and A. L. Gaeta, *Opt. Lett.* **24**, 1311-1313 (1999).

[63] C. B. Schaffer, A. Brodeur, J. F. Garcia, and E. Mazur, *Opt. Lett.* **26**, 93-95 (2001).

[64] T. N. Kim, K. Campbell, A. Groisman, D. Kleinfeld, and C. B. Schaffer, *Appl. Phys. Lett.* **86**, 201106 (2005).

[65] K. Ke, E. F. Hasselbrink Jr., and A. J. Hunt, *Anal. Chem.* **77**, 5083-5088 (2005).

[66] Y. Li, K. Itoh, W. Watanabe, K. Yamada, D. Kuroda, J. Nishii, and Y. Jiang, *Opt. Lett.* **26**, 1912-1914 (2001).

[67] M. S. Giridhar, K. Seong, A. Schülzgen, P. Khulbe, N. Peyghambarian and M. Mansuripur, *Appl. Opt.* **43**, 4584-4589 (2004).

[68] E. N. Glezer, M. Milosavljevic, L. Huang, R. J. Finlay, T. H. Her, J. P. Callan and E. Mazur, *Opt. Lett.* **21**, 2023 (1996).

[69] A. Joglekar, H. Liu, G. Spooner, E. Meyhofer, G. Mourou and A. Hunt, *Appl. Phys. B* **77**, 25 (2003).

CHAPTER 2

SILICA-GLASS CONTRIBUTION TO EFFECTIVE FIBER NONLINEARITY

[1]

In this chapter, we report on an experimental investigation of the silica-glass contribution to the effective nonlinearity of several hollow-core photonic band-gap fibers (HC-PBGF) with different air-filling fractions. We find that the silica contribution can vary over a broad range depending on small variations in fiber structure. By confining the mode to the air core, it is possible to reduce nonlinearity and loss [1]. These results are consistent with studies of the structural mechanism for light confinement within the air core [2].

Low nonlinearity is crucial for preserving the fidelity of propagating pulses, and it is important to understand the contribution from both the glass and air regions. The optical field is primarily localized in the air core, but since the nonlinear refractive index of glass is roughly 1000× larger than air, it is not obvious which medium dominates the effective nonlinearity of the fiber. It was shown [3] that the effective nonlinearity of the fundamental mode of the fiber described in Ref. [4] is approximately equal to that of the air in the fiber core. Alternatively, theoretical analysis of commercially available HC-PBGFs [5, 6] concluded that glass and air regions have comparable contributions to the total nonlinearity. Lægsgaard *et al.* [7] showed theoretically that the fraction of light that resides in the silica regions, which yields the glass contribution to total nonlinearity, depends strongly on the air-filling fraction—defined by the fractional area that air comprises within a unit cell in the holey cladding region. Recent work [8] using

[1] C. J. Hensley, D. G. Ouzounov, A. L. Gaeta, N. Venkataraman, M. T. Gallagher, and K. W. Koch, Opt. Express 15, 3507-3512 (2007).

coherent anti-Stokes Raman scattering investigated the nonlinear contribution of glass at transmission edges of the band-gap.

2.1 Self-Phase Modulation Measurements of Corning Fibers

In our experiments, we study three different fibers manufactured by Corning. Two of these fibers, Corning fiber II (CF2) and fiber III (CF3), have operational ranges centered at 1255 nm, while the third, Corning fiber I (CF1) [4], has a zero-GVD wavelength at 1425 nm with the transmission window centered at 1475 nm. Scanning electron microscope (SEM) images of the core walls (Figs. 1(b) and 1(c)) illustrate the tens of nanometers differences within the fiber profiles. The indicated widths are consistent with measurements taken around the core and along the length of the fibers to within the resolution of the SEM images. The air-filling fraction of the CF1 is 0.94, while the values for CF2 and CF3 are 0.95 and 0.96, respectively. However, as we will show, the air-filling fraction is not the sole parameter that determines the fiber nonlinearity.

The experimental setup is shown in Fig. 2. Pulses are produced by a regenerative amplification system (Hurricane, Spectra Physics) seeded by a Ti-sapphire oscillator. This 1-kHz source centered at 800 nm is used to pump an optical parametric amplifier (OPA) that supplies 100-fs pulses tunable from 1100 to 1600 nm. Using an aspheric 10× objective, the beam is coupled into the fiber, which is held inside a vacuum chamber. The coupling efficiency for all these fibers is 50% - 55%. We couple 100-fs pulses at the zero-GVD wavelength (1255 nm for CF2 and CF3 and 1425 nm for CF1) and measure the output pulse spectrum and autocorrelation when the fiber holes are filled with air and when the chamber is

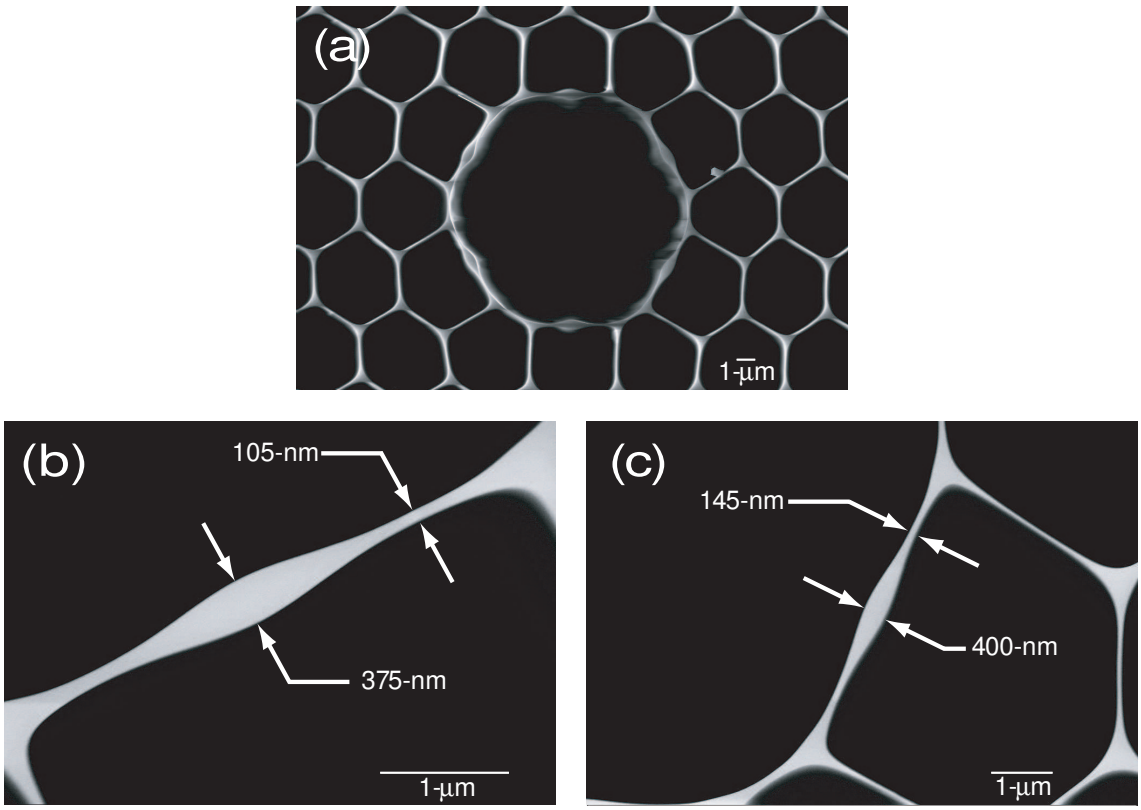

Figure 2.1: (a) SEM image of Corning fiber I. All three fibers characterized in this work have this same general structure. Closeup SEM of air-core wall of Corning fiber II (b) and Corning fiber III (c). Indicated dimensions have an error of ±5 nm.

evacuated to a pressure less than 30 mTorr.

In an effort to calibrate our results to previously reported data, Fig. 3(a) shows the transmitted pulse spectrum for the commercially available HC-800-01 fiber. For 100-nJ pulses propagating through the air-filled fiber, the spectrum is nearly identical to that of 200-nJ pulses propagating in vacuum, indicating that the silica-glass structure and air have nearly equal contributions to the effective fiber nonlinearity, which is in good agreement with the theoretical results of Ref. [5]. The pulses of the regenerative system used in these measurements carry a small negative chirp, which explains the spectral narrowing of the out-

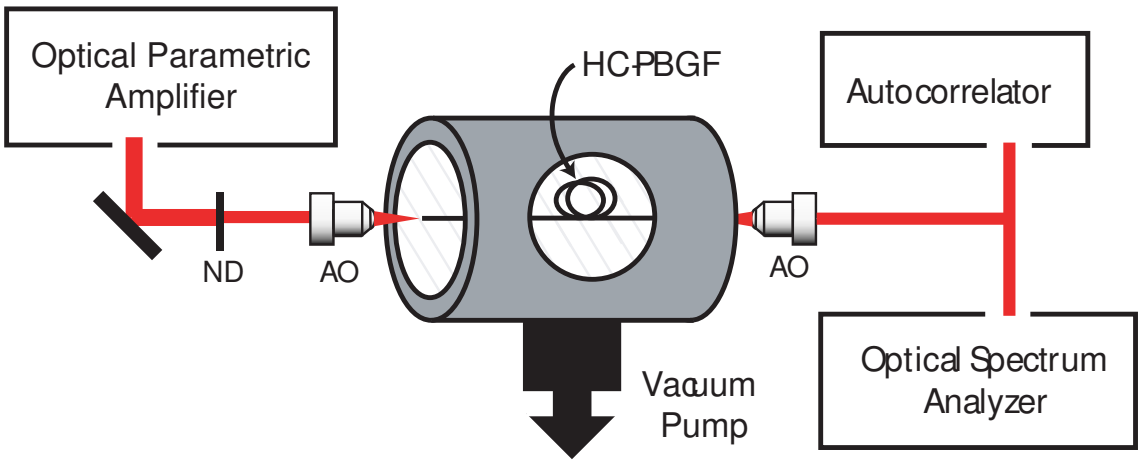

Figure 2.2: Experimental setup showing the beam from the femtosecond optical parametric amplifier attenuated by neutral density filters (ND) and then coupled in and out of the hollow-core photonic band-gap fiber (HC-PBGF) by two 10× aspheric objectives (AO).

put pulse spectra [9]. Fig. 3(b) shows the output spectrum for 2-μJ pulses propagating through the evacuated core of CF1. The absence of structure or spectral broadening at these high pulse energies indicates that the fiber nonlinearity is dominated by air. It has been shown that 900-nJ, 110-fs pulses in an air-filled core undergo significant soliton self-frequency shifting due to Raman scattering [3].

2.2 Nonlinear Schrodinger Equation Simulations

To quantify better the glass contribution to the total nonlinearity, we simulated pulse propagation with the generalized nonlinear Schrodinger equation, which includes third- and fourth-order dispersion, and self-steepening [10]. This method has recently been used to investigate nonlinearity in fs-written

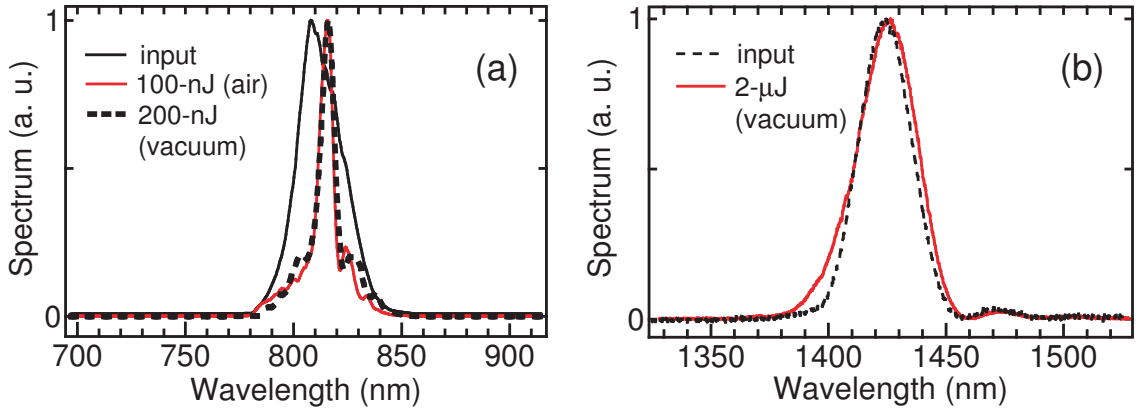

Figure 2.3: (a) Output spectra for energies of pulses propagating in air and vacuum in the HC-800-01 fiber that produces nearly identical spectral shapes. (b) Output spectrum for a pulse with an energy of 2 μJ propagating in vacuum for Corning fiber I.

waveguides [11]. In our simulations we define the relative intensity η in silica as the fraction of the peak field intensity I_{silica} in the silica glass to that I_{core} in the hollow-core, that is, $\eta = I_{silica}/I_{core}$.

For an evacuated fiber, we use the nonlinear length definition [12] and solve for the total effective nonlinearity,

$$L_{NL} = \frac{\lambda}{2\pi n_2 I_o^{silica}} = \frac{\lambda}{2\pi n_2 \eta I_o^{core}} = \frac{1}{\gamma_{eff} P_o^{core}}. \tag{2.1}$$

Here $\gamma_{eff} = \eta 2\pi n_2/\lambda A_{eff}$ is the total effective nonlinearity, $n_2 = 2.6\times10^{-16}$ cm^2/W is the nonlinear refractive index of silica, A_{eff} is the mode field area (~70-μm^2 for all these fibers), and λ is the wavelength. In our simulations η is varied until the best fit of theory to the measured output spectrum is achieved.

By this method, we find that the relative intensity in silica for CF1 is 0.015% (Fig. 4). To obtain the best agreement, we used a slightly larger value for the

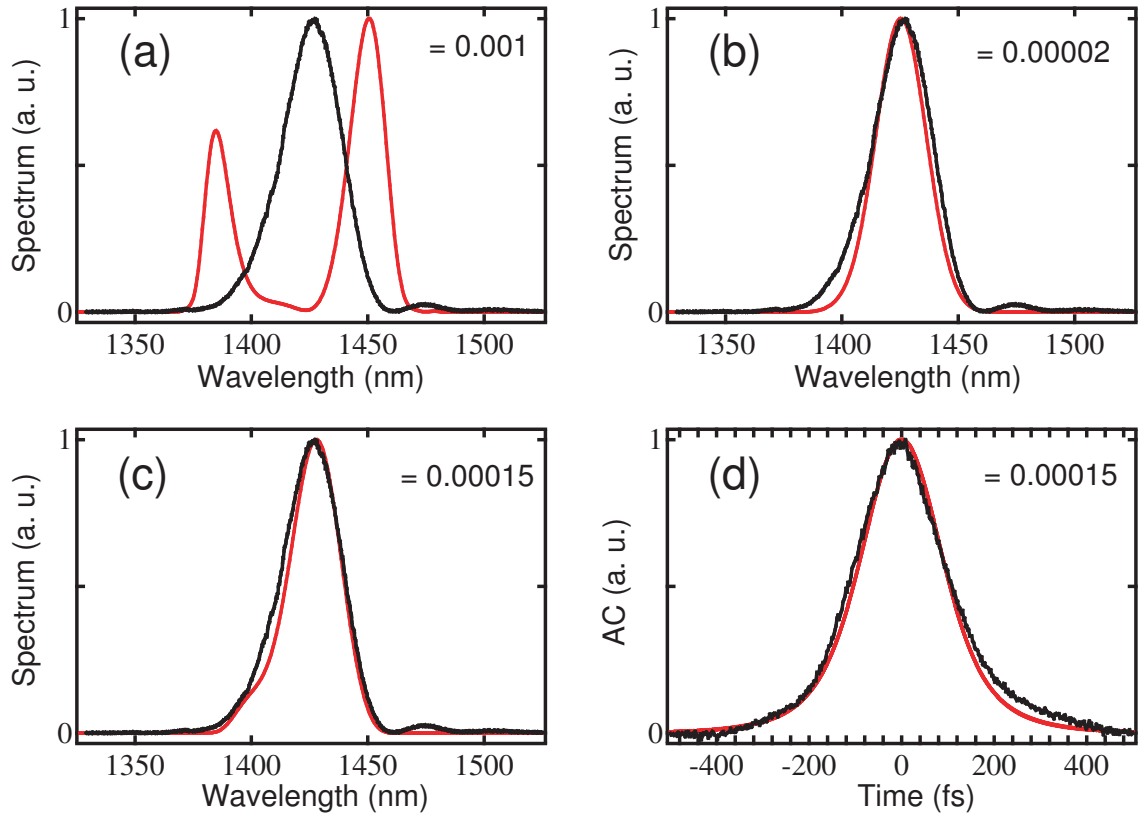

Figure 2.4: Several iterations are shown to produce the best numerical fit (red) for the experimental output spectrum (black) for a 2.054-μJ pulse energy in Corning fiber I [(a)-(c)]. In addition, we show the numerical best fit (red) and experimental (black) output autocorrelation (d).

third-order dispersion than that reported [3]. Repeating this process of varying η in our simulation to fit the measured output spectra for CF2 and CF3 yields relative intensities of 0.10% and 0.042%, respectively. Thus the glass contribution to the effective nonlinearity of CF1 is approximately 7× smaller than that of CF2 and 3× smaller than that of CF3. The resulting total effective nonlinearities γ_{eff} are summarized below in Table 1, and for comparison we have listed the value for standard step-index fiber (SMF-28). In the final column we have also included the case for the air-filled fiber at 1 atm with $n_2^{air} = 5.0 \times 10^{-19}$ cm^2/W

[13].

Table 2.1: Effective fiber nonlinearity γ_{eff}, for various fibers.

	γ_{eff} (W^{-1}/cm)	
Fiber type	Evacuated core	Air-filled core
Corning fiber I	2.4×10^{-9}	3.4×10^{-8}
Corning fiber II	1.9×10^{-8}	5.4×10^{-8}
Corning fiber III	7.7×10^{-9}	4.3×10^{-8}
Step-index fiber	5×10^{-5}	

2.3 Nanometer Structural Changes and Fiber Nonlinearity

As a final demonstration of this structurally sensitive nonlinearity, we measure the spectral broadening of the output pulse as a function of pulse energy (see Fig. 5). For this experiment, transform-limited pulses are coupled into evacuated fibers at the zero-dispersion wavelength. Under these conditions, changes to the spectral full-width-at-half-maximum are attributed entirely to the nonlinearity of the fiber [12]. These results are consistent with our previous data showing that similar broadening occurs at lower peak powers for CF2 due to the greater contribution of silica glass to the total nonlinearity in this fiber (Fig. 5).

In conclusion, we determine experimentally the silica-glass contribution to the effective nonlinearity of three hollow-core photonic band-gap fibers. We

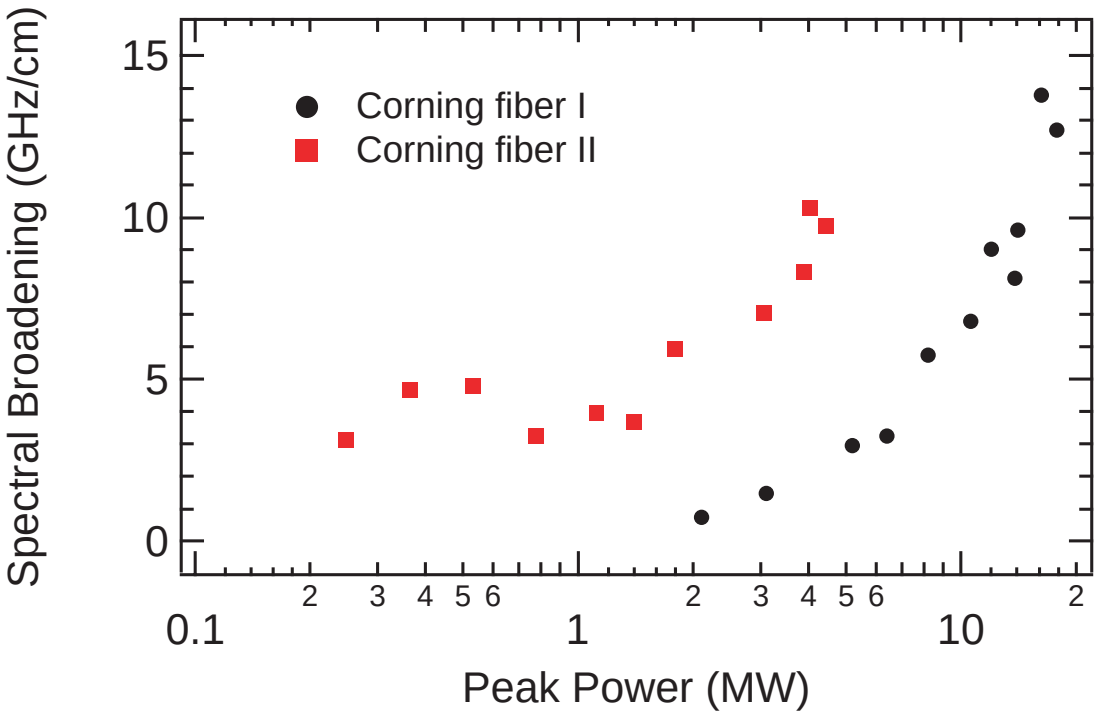

Figure 2.5: Output pulse spectral broadening per unit fiber length for Corning fiber I (circles) and fiber II (squares).

find that the relative power in the silica—normalized to that in the air-core region—can vary by nearly an order of magnitude and is highly sensitive to the fiber structure. As a result, the contribution of silica glass to the effective fiber nonlinearity, and thus to the total nonlinearity, can be engineered over broad limits through small structural changes. These results are relevant to applications involving delivery of high-power pulses, where by evacuating the fiber core the majority of the fiber nonlinearity can be eliminated.

REFERENCES

[1] J. A. West, C. M. Smith, N. F. Borrelli, D. C. Allan and K. W. Koch, *Opt. Express* **12**, 1485-1496 (2004).

[2] P. J. Roberts, D. P. Williams, B. J. Mangan, H. Sabert, F. Couny, W. J. Wadsworth, T. A. Birks, J. C. Knight and P. St. J. Russell, *Opt. Express* **13**, 8277-8285 (2005).

[3] D. G. Ouzounov, F. R. Ahmad, D. Muller, N. Venkataraman, M. T. Gallagher, M. G. Thomas, J. Silcox, K. W. Koch, and A. L. Gaeta, *Science* **301**, 1702-1704 (2003).

[4] C. M. Smith, N. Venkataraman, M. T. Gallagher, D. Muller, J. A. West, N. F. Borrelli, D. C. Allan, and K. W. Koch, *Nature* **424**, 657-659 (2003).

[5] F. Luan, J. C. Knight, P. St. J. Russell, S. Campbell, D. Xiao, D. T. Reid, B. J. Mangan, D. P. Williams and P. J. Roberts, *Opt. Express* **12**, 835-840 (2004).

[6] G. Humbert, J. C. Knight, G. Bouwmans, P. St. J. Russell, D. P. Williams, P. J. Roberts, B. J. Mangan, *Opt. Express* **12**, 1477-1484 (2004).

[7] J. Lægsgaard, N. A. Mortensen, J. Riishede and A. Bjarklev, *J. Opt. Soc. Am. B* **20**, 2046-2051 (2003).

[8] I. V. Fedotov, A. B. Fedotov, and A. M. Zheltikov, *Opt. Lett.* **31**, 2604-2606 (2006).

[9] M. Oberthaler and R. A. Höpfel, *Appl. Phys. Lett.* **63**, 1017-1019 (1993).

[10] T. Brabec and F. Krausz, *Phys. Rev. Lett.* **78**, 3282-3285 (1997).

[11] D. Blömer, A. Szameit, F. Dreisow, T. Schreiber, S. Nolte and A. Tünnermann, *Opt. Express* **14**, 2151-2157 (2006).

[12] G. P. Agrawal, *Nonlinear Fiber Optics* (Academic Press, 1989).

[13] R. W. Boyd, *Nonlinear Optics* (Academic Press, ed. 2, 2003).

CHAPTER 3

LOW-LOSS COUPLING OF FEMTOSECOND LASER PULSES

[1]

In this chapter we investigate the transmission of linearly-, radially- and azimuthally-polarized (RP and AP) beams in HC-PBGF with femtosecond laser pulses. Previous work has studied damage in these fibers at nanosecond pulse lengths [1, 2, 3, 4], with delivered pulse energies reaching 370 μJ [2], but to the best of our knowledge, there has been no formal study in the femtosecond regime. The ability to excite ultrafast phase or polarization vortices in these fibers could be interesting for studying various nonlinear effects in gas-filled fibers and for intense beam delivery applications.

3.1 Radial and Azimuthal Beams

Optical polarization vortices display intriguing properties both in the linear and nonlinear propagation regimes. The basic form of polarization vortices is a purely radially or azimuthally polarized (RP or AP) beam with a Laguerre-Gaussian TEM_{01} ring-shaped intensity distribution and a polarization singularity at the center. These basic polarization vortices can also be described as a superposition of two-phase vortices with opposite circular polarization and helicity. In the linear paraxial propagation regime, these beams are eigenmodes of both free space and cylindrical waveguides. Under tight-focusing conditions, the RP (AP) beams produce strong longitudinal electric- (magnetic-) field

[1] A. A. Ishaaya, C. J. Hensley, B. Shim, S. Schrauth, K. W. Koch and A. L. Gaeta, in preparation.

components at the focus [5], which could be beneficial for various applications such as trapping and acceleration of particles [6, 7], microscopy [8], and laser processing [5]. In the nonlinear optical regime, a few theoretical and experimental studies with RP and AP beams have been reported, which include vortex-driven surface second-harmonic generation [6], propagation in Kerr-type medium [9, 10, 11, 12], and theoretical work on RP and AP dark solitons in defocusing Kerr media [13].

Generation of RP and AP beams was demonstrated by a variety of methods. These include coherently combining two linearly polarized degenerate LG beams [14], coherently combining two circularly polarized phase vortices [14], exploiting special laser resonator schemes [15, 16], using a segmented wave plates [8, 17], liquid crystals [18], holographic elements [19], sub-wavelength gratings [20], and selective excitation in fibers [21]. These methods differ in their complexity, efficiency, mode purity, and power handling capability. So far excitation of RP and AP modes in optical fibers has been pursued mainly with low power CW lasers and standard step index fibers [21, 22, 23]. Recent results have demonstrated coupling into HC-PBGF using CW generated optical vortices [24].

3.2 Efficient Coupling with Linear Polarization

We first investigate the maximum coupling and damage threshold of these fibers with linearly polarized Gaussian beams. Typical damage in coupling from free space into a HC-PBGF with femtosecond laser pulses is shown in Fig. 3.1b. Mismatching the mode size or shape of the incoming laser beam with that of the

HC-PBGF causes this catastrophic interaction. To minimize this, careful measures are taken to match the mode profile of the fiber used in this experiment. This procedure drastically increased the coupling efficiency into the HC-PBGF and resulted in higher peak intensity within the fiber core prior to optical breakdown.

The HC-PBGF used in this investigation (Crystal Fibre, HC-800-02, Fig. 3.1a) operates at a center wavelength of 835 nm and exhibits an attenuation of 0.25 dB/m for a 70-nm region surrounding that wavelength. This fiber has a core diameter of 6.8 μm and a measured mode-field diameter (1/e-width) of 5.0 μm. In addition, and important for this particular investigation, is that the fundamental mode exhibits a strong Gaussian shape to the fundamental mode allowing for appropriate mode matching with standard optics.

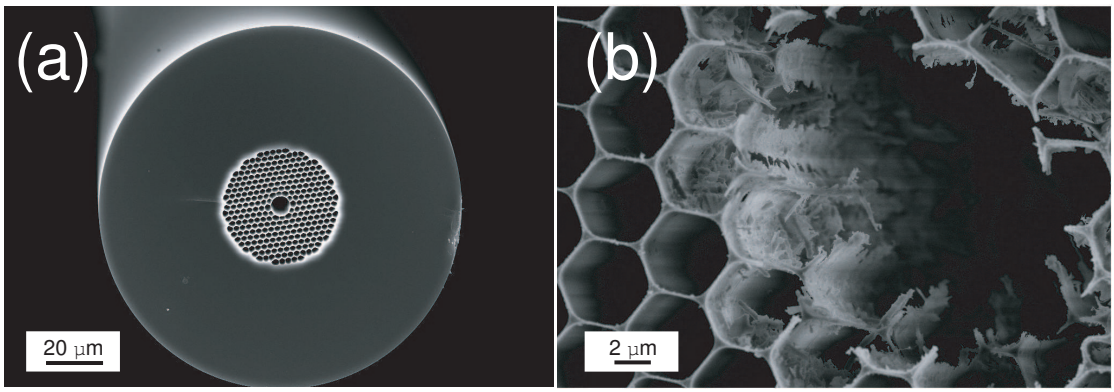

Figure 3.1: (a) SEM image of HC-800-02 fiber (Crystal Fibre) used in this experiment and (b) damage that occurred when a high pulse energy, mismatched mode is coupled into a similar fiber designed to operate at 1550-nm center wavelength

For this experiment we used an amplified Ti:Sapphire laser (Coherent Hydra) operating at 1-kHz repetition rate, producing 40-fs pulses, centered at 810 nm, and capable of 1-mJ pulse energies. The setup for this work is shown in Figure 3.2. After passing through an aperture, the amplified laser is spatially fil-

tered and then attenuated using a combination of quarter- and half-wave plates followed by a thin-film polarizer. Coupling in and out is performed with a pair of 16× (0.25 NA) aspheric lenses with the 30-cm length of fiber mounted on three-axis flexure stages. To match the mode of the HC-PBGF, the aperture size and position of L2 are adjusted in an iterative process to produce the highest coupling. In order to avoid damaging the front face of the fiber, the initial coupling uses relatively low pulse energies (~2 nJ), which are then increased once the fundamental mode is properly excited.

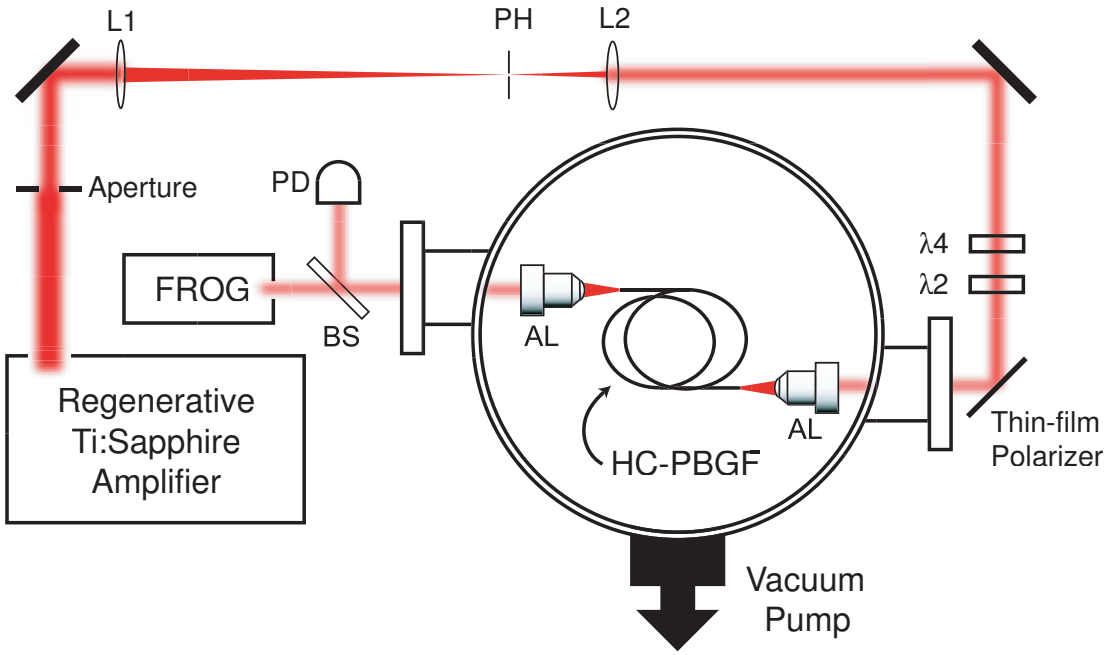

Figure 3.2: Experimental setup for linear polarization studies. An amplified Ti:sapphire system is spatially filtered and then coupled into the HC-800-02 fiber using a pair of aspheric lenses (AL) held inside an evacuated chamber.

3.3 Linear Polarization Damage Threshold

In order to measure coupling with optimal mode matching, we operated with pulse energies well below damage threshold for this fiber and without the vacuum chamber shown in Figure 3.2. Using 100-nJ pulses we achieve 98% coupling, which to our knowledge, is the highest value observed in HC-PBGF when accounting for transmission loss of the fiber. At higher pulse energies, the three-axis stages and fiber are placed inside of a chamber and evacuated to a pressure of 5 mtorr to avoid ionization effects. The results of this work are shown in Figure 3.3 where we have plotted input pulse energy at the face of the fiber and output energy as measured at the back end of the fiber. The actual experimental coupling achieved inside the chamber was reduced to 93.5%, as shown in the plot. We attribute this reduction of coupling as compared to the lower energy results outside the chamber to distortions of the beam caused by the chamber windows. As shown in the plot (Figure 3.3), the highest measured pulse energy at the output was 1.8 μJ, which for a 40-fs pulse corresponds to a peak intensity of 1.6×10^{14} W/cm^2 and is, to our knowledge, is the highest peak intensity observed inside a hollow-core photonic band-gap fiber. To verify that the fidelity of the pulse is maintained during transmission through the evacuated fiber, a frequency-resolved optical gating (FROG) measurement [25] of the input and output of the fiber is shown in Figure 3.4. The observed broadening of the pulse width is consistent with the combined dispersion of the waveguide and the two 3-mm thick Sapphire windows on the vacuum chamber.

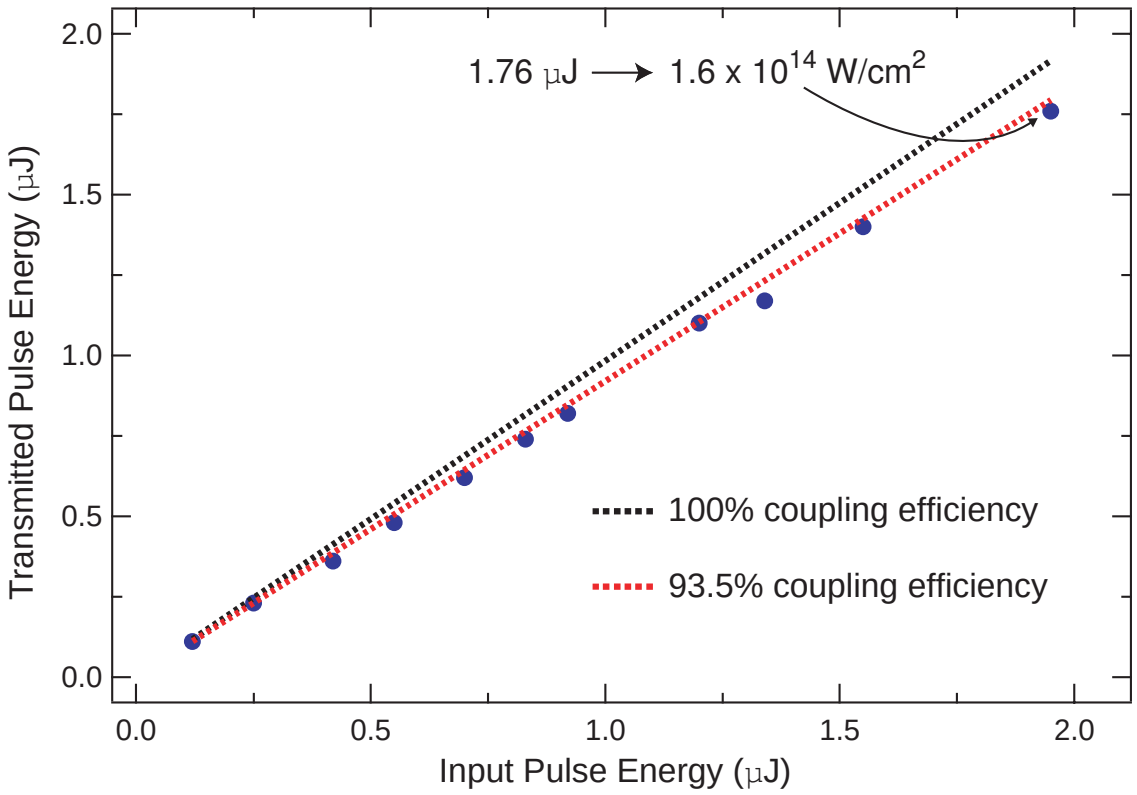

Figure 3.3: Transmitted pulse energy through a 30-cm length of evacuated HC-800-02 fiber as a function of input pulse energy.

3.4 Transmission of Polarization Vortices

For the polarization vortices studies the experimental setup is shown in Figure 3.5. The output of a Ti:Sapphire laser oscillator (80-MHz repetition rate, 50-fs pulses, centered at 810 nm) is converted into a linearly-polarized degenerate TEM_{01} Laguerre-Gaussian beam using a 0-π phase plate and a spatial filter. The beam is then split into two arms, where one is rotated by 90 degrees with a periscope, before being interferometrically recombined with the other to achieve a RP beam. Time and phase alignment is achieved by controlling the delay with a high-precision stage. An AP beam is obtained by rotating the phase plate by 90 degrees. This beam is then focused with a 10× (0.16 NA) aspheric lens into

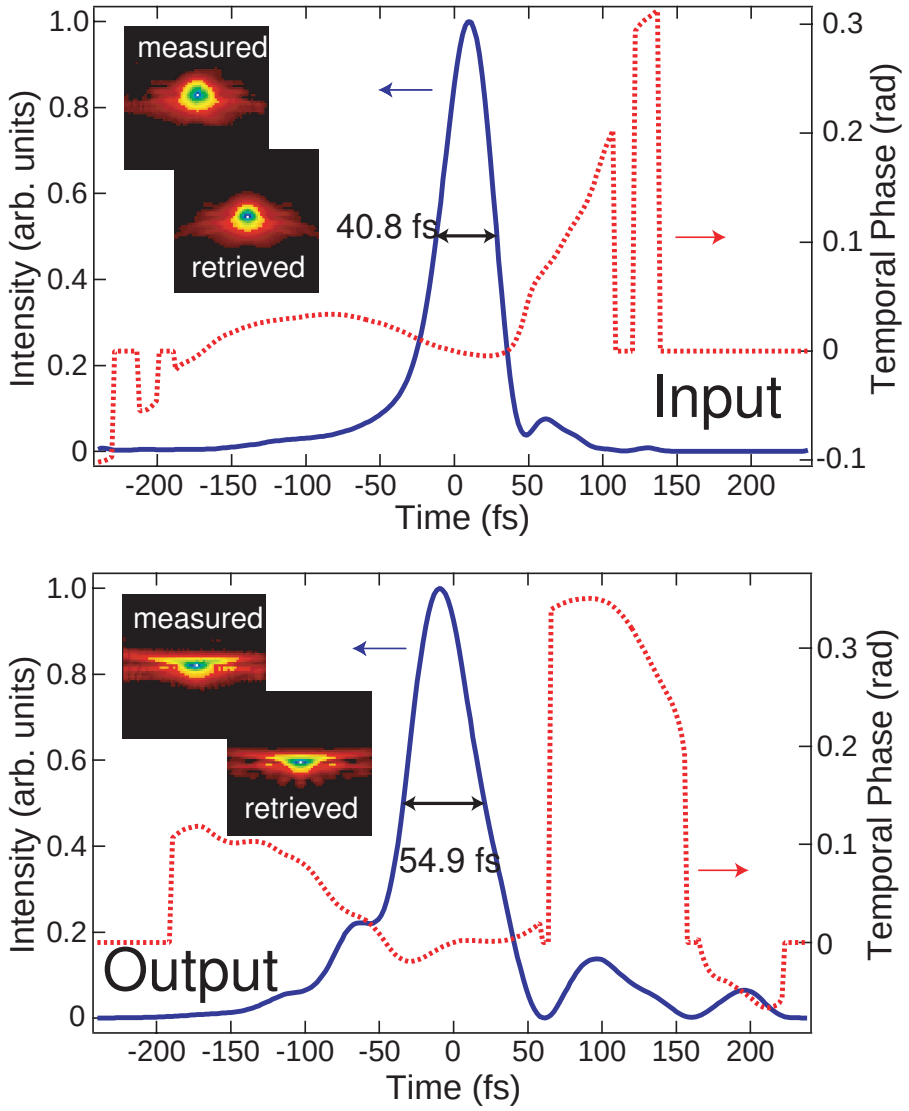

Figure 3.4: Retrieved temporal profiles from the FROG measurements of the input (top) and output (bottom) pulses.

a 20-cm length of commercially available HC-PBGF (Crystal Fibre, HC-800-01). The fiber core is hexagonal with a total width of 9.2 μm and 9.5 μm along the short and long axes, respectively. The output face of the fiber is imaged onto a 12-bit CCD with either a 10× or a 40× aspheric objective.

The measured intensity distributions of the RP beam before the fiber are shown in Figure 3.6(a-e). The beam has the expected TEM_{01} donut shape, and

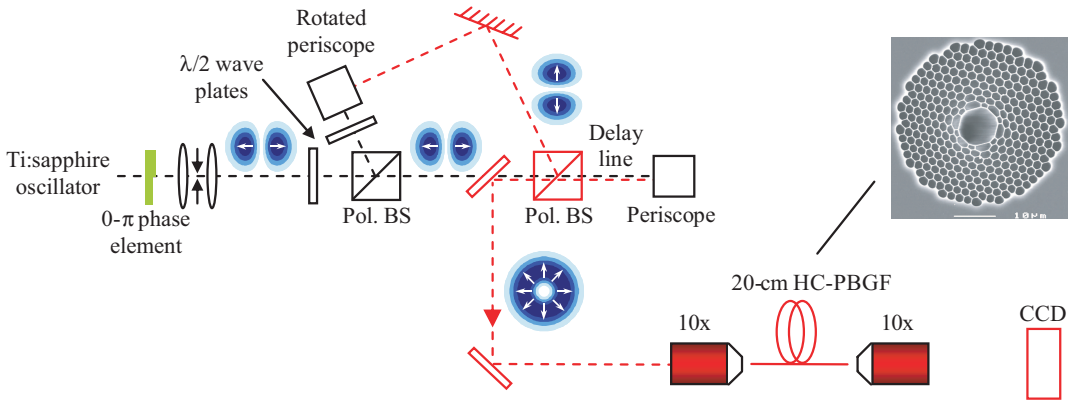

Figure 3.5: Experimental setup for the vortices studies. A linearly-polarized Gaussian beam from a Ti:sapphire oscillator is converted to a radially- or azimuthally-polarized donut beam and then focused into the HC-PBGF. Elements in red are in a different plane.

the two-lobe pattern formed after passing through a polarizer rotates according to the angular position of the polarizer, which is indicative of radial polarization. The corresponding measured intensity distributions just after the output face of the fiber are shown in Figure 3.6(f-j), and it is evident that the beam maintains its donut shape and its radial polarization. Figure 3.7 shows the intensity distribution precisely at the output face of the fiber. Altering the input polarization of the beam by slightly changing the time alignment of the two arms has a minor effect on the output.

The effective transmission of the RP beam through the fiber, including the coupling losses, was measured to be 91%, which we believe to be the highest efficiency reported so far for the excitation of a RP beam in any optical fiber with ultrafast pulses. All the experiments were conducted at fiber input pulse energies between 0.75 and 62.5 pJ.

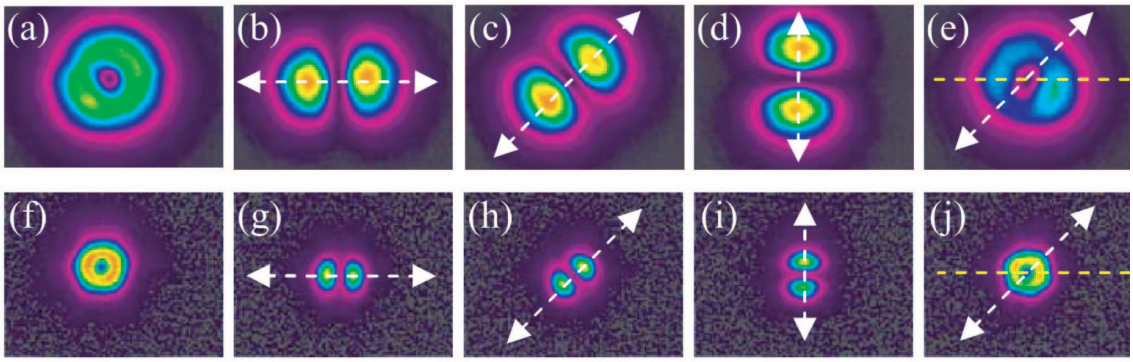

Figure 3.6: Experimental intensity distributions of a RP beam before and after the PBGF. [(a)-(e)] Intensity distributions in front of the focusing objective; [(f)-(j)] Intensity distributions just after the fiber output face. White arrows indicate the orientation of a linear polarizer placed before the CCD, and the yellow dashed line indicates the fast axis of a quarter wave plate placed before the polarizer. Color scale is different for each image, where red (blue) represents high (low) intensity.

When trying to excite the hybrid radial-azimuthal donut modes by applying a $\pi/2$ phase shift to one arm, the output intensity distribution deteriorates (nonzero intensity at the center), indicating a non-pure mode at the output. When the input beam is AP, we observe azimuthal polarization at the output of the fiber, but the mode is also less pure. Figure 3.8 shows the output intensity distributions in the case of input azimuthal polarization. Instead of a donut shape with zero intensity at the center, we observe a circular distribution with a slight dip at the center and after passing through a polarizer, the lobes are slightly rotated compared to their expected position. Thus, in this specific fiber, we observe a clear tendency for support of radial polarization over azimuthal polarization.

The discrimination between radial and azimuthal polarization in this fiber could originate from the non-perfect cylindrical cross-section of the fiber. Figure 9 shows the typical near-field intensity distribution from the fiber as advertised

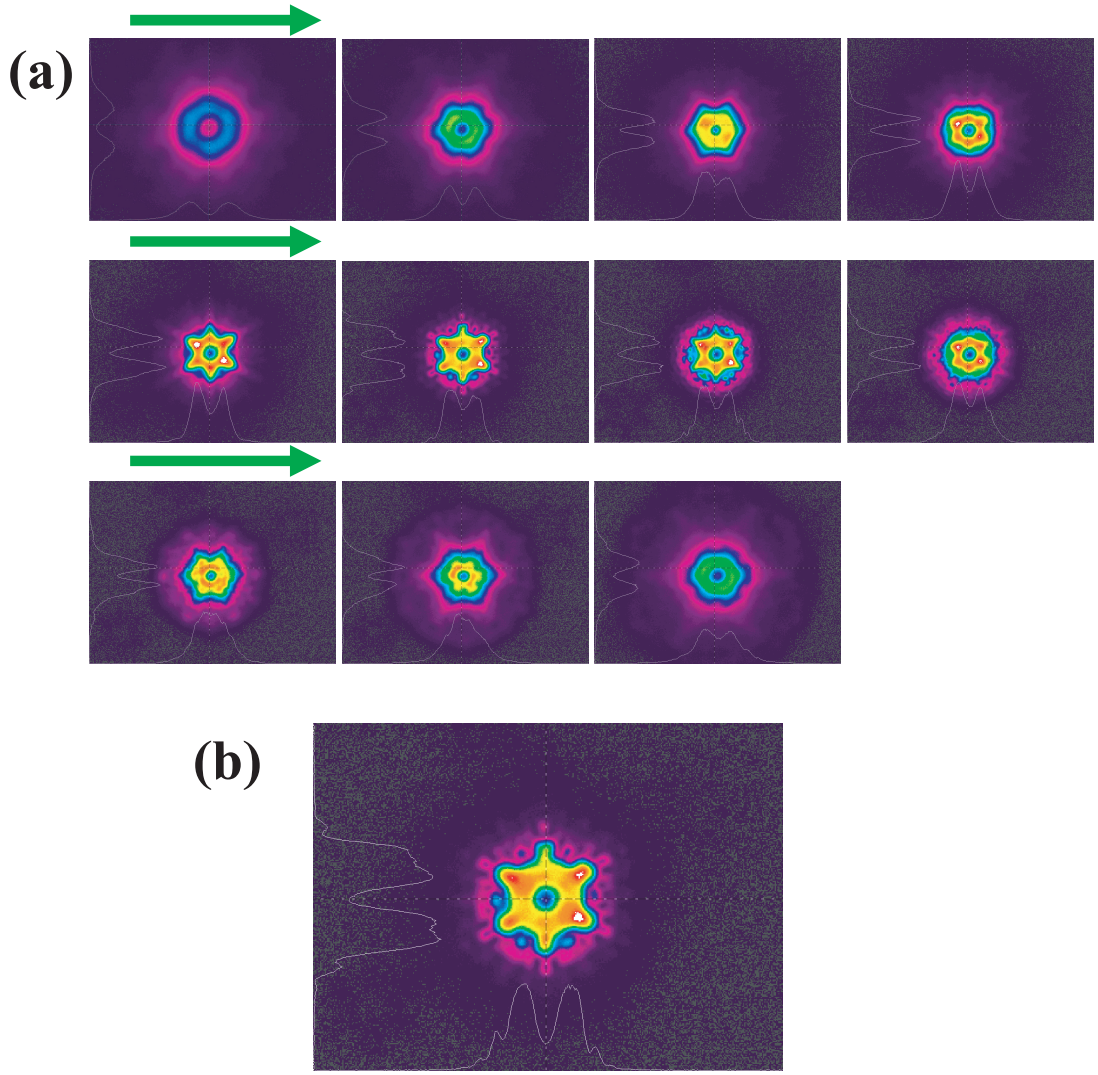

Figure 3.7: Experimental intensity distributions of the radially polarized beam at the PBGF output face region. (a) The intensity distribution detected by the CCD camera as the 40x objective is moved towards the fiber tip; (b) the intensity distribution exactly at the fiber output face.

in the data sheet. The distribution is not radially symmetric and is characterized by two different widths. This can result in larger losses or scattering for the azimuthal polarization versus the radial polarization.

For the linearly polarized mode we measure a peak transmitted intensity of

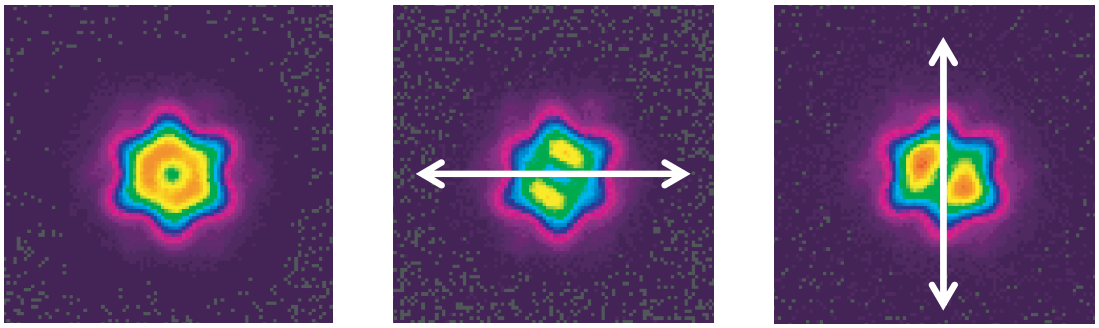

Figure 3.8: Experimental intensity distributions of AP beam after the HC-PBGF. The white arrows indicate the orientation of a linear polarizer placed before the CCD. Color scale is different for each image, where red (blue) represents high (low) intensity.

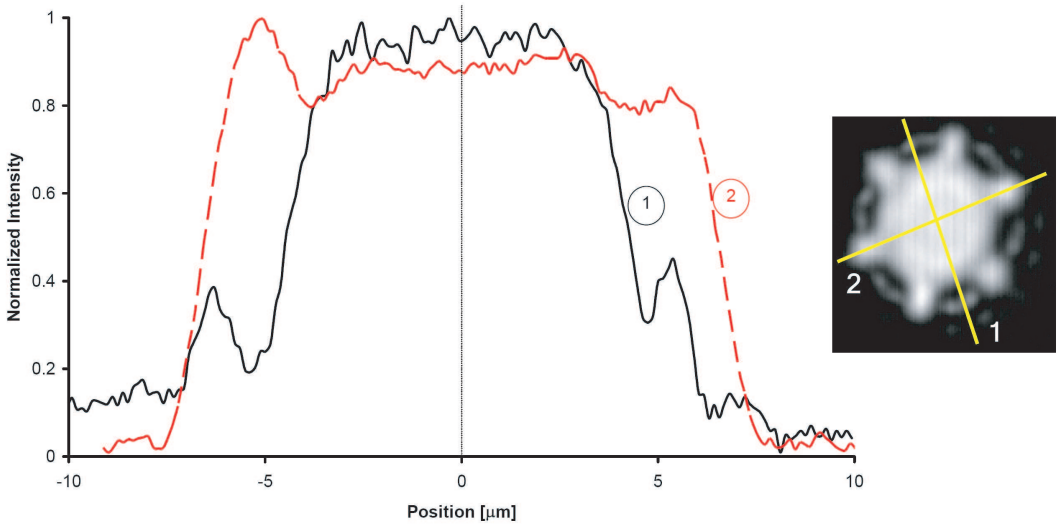

Figure 3.9: Typical near-field intensity distribution from a HC-800-01 fiber, as published by the manufacturer (Crystal Fibre datasheet, [HC-800-01])

1.6×10^{14} W/cm^2 using 40-fs pulses and a coupling efficiency of 98%, while for the radially polarized mode we find a 91% coupling efficiency, both of which are the highest to our knowledge. In addition, we have demonstrated experimentally that ultrafast laser pulses with pure radial polarization can be efficiently coupled into a HC-PBGF. In contrast to the radial the azimuthal suffers degra-

dation along the fiber and does not maintain its polarization. Though the reason behind this is not clear, we believe the preference of radial polarization is due to the non-perfect cylindrical cross section of the fiber. This low-loss coupling of linear and radial polarization beams should extend the capabilities of these fibers for studying intense nonlinear light-gas interactions and beam delivery of high peak power femtosecond laser pulses.

REFERENCES

[1] G. Humbert, J. C. Knight, G. Bouwmans, P. St. J. Russell, D. P. Williams, P. J. Roberts and B. J. Mangan, *Opt. Express* **12**, 1477-1484 (2004).

[2] J. D. Shephard, J. D. C. Jones, D. P. Hand, G. Bouwans, J. C. Knight, P. St. J. Russell and B. J. Mangan, *Opt. Express* **12**, 717-723 (2004).

[3] L. Michaille, D. M. Taylor, C. R. Bennett, T. J. Shepherd, C. Jacobsen, and T. P. Hansen, *Proc. SPIE* **5618**, 30-38 (2004).

[4] J. Tauer, F. Orban, H. Kofler, A. B. Fedotov, I. V. Fedotov, V. P. Mitrokhin, A. M. Zheltikov and E. Wintner, *Laser Phys. Lett.* **4**, 444-448 (2007).

[5] L. Novotny, M.R. Beversluis, K. S. Youngworth, and T. G. Brown, *Phys. Rev. Lett.* **86**, 5251 (2001).

[6] M. O. Scully, *Appl. Phys. B* **51**, 238 (1990).

[7] E. J. Bochove, G. T. Moore, and M. O. Scully, *Phys. Rev. A* **46**, 6640 (1992).

[8] R. Dorn, S. Quabis, and G. Leuchs, *Phys. Rev. Lett.* **91**, 233901 (2003).

[9] D. Pohl, *Phys. Rev. A* **5**, 1906 (1972).

[10] J. W. Haus, Z. Mozumder, and Q. Zhan, *Opt. Express* **14**, 4757 (2006).

[11] A. A. Ishaaya, L. T. Vuong, T. D. Grow and A. L. Gaeta, *Opt. Lett.* **33**, 13-15 (2008).

[12] L. T. Vuong, A. A. Ishaaya, T. D. Grow, A. L. Gaeta, and E. R. Eliel, *Frontiers in Optics, OSA Technical Digest* (CD) (Optical Society of America, 2006), paper FThP3.

[13] A. Ciattoni, B. Crosignani, P. Di Porto, and A. Yariv, *Phys. Rev. Lett.* **94**, 073902 (2005).

[14] S. C. Tidwell, D. H. Ford, and W. D. Kimura, *Appl. Optics* **29**, 2234-2239 (1990).

[15] R. Oron, S. Blit, N. Davidson, A. A. Friesem, Z. Bomzon, and E. Hasman, *Appl. Phys. Lett.* **77**, 3322-3324 (2000).

[16] I. Moshe, S. Jackel, and A. Meir, *Opt. Lett.* 28, 807-809 (2003).

[17] G. Machavariani, Y. Lumer, I. Moshe, A. Meir, and S. Jackel, *Opt. Lett.* **32**, 1468-1470 (2007).

[18] M. Stalder and M. Schadt, *Opt. Lett.* **21**, 1948 (1996).

[19] E. Churin, J. Hosfeld, and T. Tschudi, *Opt. Commun.* **99**, 13-17 (1993).

[20] Z. Bomzon, G. Biener, V. Kleiner, and E. Hasman, *Opt. Lett.* **27**, 285-287 (2002).

[21] T. Grosjean, A. Sabac and D. Courjon, *Opt. Commun.* **252**, 12 (2005).

[22] G. Volpe and D. Petrov, *Opt. Commun.* **237**, 89 (2004).

[23] J. Li, K. Ueda, M. Musha, A. Shirakawa and L. Zhong, *Opt. Lett.* **31**, 2969 (2006).

[24] T. G. Euser, G. Whyte, M. Scharrer, J. S. Y. Chen, A. Abdolvand, J. Nold, C. F. Kaminski and P. St. J. Russell, *Opt. Express* **16**, 17972-19781 (2008).

[25] D. Kane and R. Trebino, *IEEE J. Quantum Electron.* **29** (2), 571 (1993).

CHAPTER 4

FIBER GAS CELL FABRICATED USING FEMTOSECOND MICROMACHINING

[1]

In this chapter, we present a noninvasive approach to filling and evacuating hollow-core photonic band-gap fiber (HC-PBGF) via a micrometer-sized channel drilled through the fiber wall with focused femtosecond laser pulses. With this process a very compact, low-loss, fiber gas cell can be produced by splicing the ends of the HC-PBGF to step-index fiber. The section of the fiber containing the microchannel is sealed with epoxy in a small vacuum chamber, with the remaining fiber exposed allowing for easy manipulation and light coupling. This HC-PBGF gas cell can then be evacuated and filled with gas at pressures both far below and far above one atmosphere.

Many of the novel applications using HC-PBGF described in chapter 1 require the introduction of a gas medium into the fiber core. Typically in these experiments, the fiber is enclosed in a vacuum cell and light is coupled in and out of the fiber through windows with microscope objectives. Recent work [1, 2], has focused on creating all-fiber gas cells using HC-PBGFs. However, a compact system that allows for variable filling of fibers over a wide range of pressures has yet to be achieved.

[1] C. J. Hensley, D. H. Broaddus, C. B. Schaffer, and A. L. Gaeta, Opt. Express 15, 6690-6695 (2007).

4.1 Material Removal in Hollow-Core PBGF

The system used for drilling is a commercial, regeneratively amplified Ti:Sapphire laser (Spectra-Physics, Hurricane) capable of producing 90-fs, 1-mJ, 800-nm pulses, at a 1-kHz repetition rate. These pulses are focused through a Zeiss Neofluar 0.9-NA multi-immersion objective onto the fiber. This objective has a correction collar designed for use with immersion oil, water, and glycerine, which has an index of refraction similar to that of fused silica. The fiber is held in index-matching fluid ($n = 1.45$) and translated through the focus of the objective at a rate of 1 μm/s using a Newport PM-500 stage at 100-nm step sizes. The index-matching fluid acts both to reduce aberrations from tightly focusing into the cylindrical fiber and to assist with debris removal by wicking into the forming capillary. Circularly-polarized light is used to produce a more rounded hole through the fiber [3]. As an initial proof-of-principle demonstration, a microchannel is created in a Corning SMF-28E fiber. By translating the step-index fiber upward through the laser focus, drilling is performed from the surface toward the core of the fiber. The threshold energy for surface void formation is found to be ~50 nJ. Microchannel formation in conventional step-index fiber with femtosecond laser-irradiation followed by etching has previously been demonstrated for potential sensing applications [4].

The presence of multiple glass-air interfaces poses a problem in transferring this method to laser drilling through a HC-PBGF. To overcome the scattering and optical aberrations due to these surfaces, index-matching fluid is continuously pumped through the core and the surrounding capillaries of the fiber during the laser drilling. This fluid flow has the added benefit of removing debris within the fiber core and the surrounding capillary structure. To take advantage

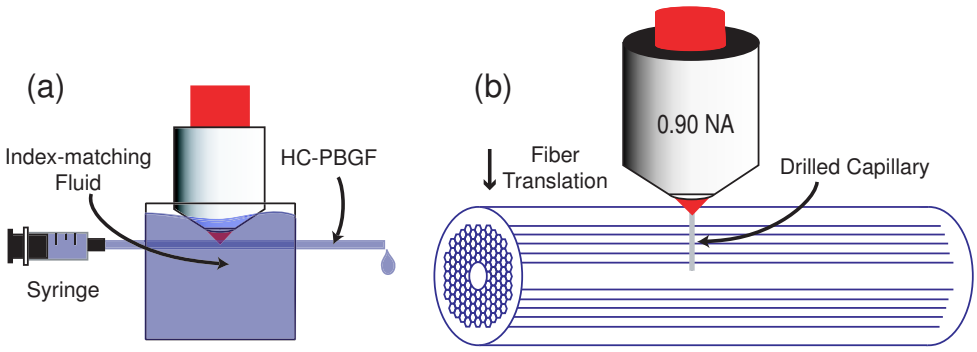

Figure 4.1: (a) Experimental setup for laser-drilling. (b) Schematic showing the drilling orientation for HC-PBGF.

of this flowing removal of debris, laser-drilling in the HC-PBGF is performed from the core to the surface (Fig. 4.1), so that any ejected debris is swept down the capillaries and out of the fiber. After drilling, the index-matching fluid is removed by flushing the air-core and surrounding capillaries multiple times with methanol and nitrogen gas, which re-establishes optical transmission through the fiber. To determine the threshold energy required for vacancy formation, a series of holes are drilled into a single length of HC-PBGF. SEM images of entry holes produced with pulse energies between 50 and 280 nJ show little increase in hole diameter with pulse energy. However, by imaging the fluid-filled fiber perpendicular to the drilling axis during the drilling, additional structural damage is observed to occur at higher pulse energies. Minimizing the energy required to form a microchannel in the HC-PBGF reduces the impact on optical transmission caused by this collateral damage within the guiding structure. In the work presented here, all channels are drilled with 80-nJ pulse energy, which is slightly above threshold for void formation (Fig. 4.2).

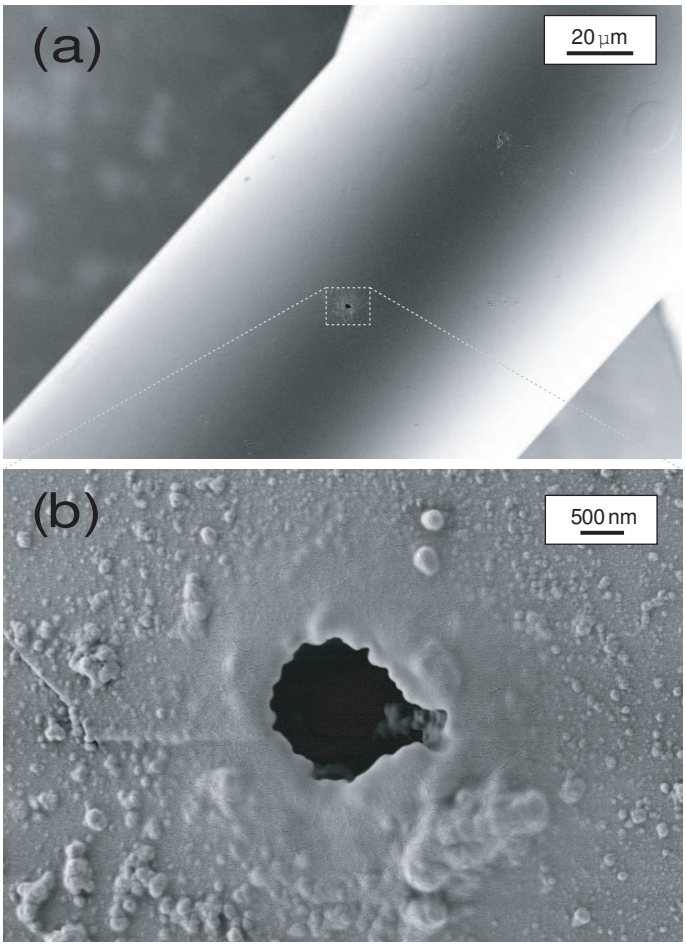

Figure 4.2: (a) SEM image of HC-1550-02 fiber laser drilled with 80-nJ pulses. (b) Closeup image of drilled capillary formed in the side of fiber, the surface diameter of the channel is 1.5 μm.

4.2 Microchannel Drilling in 800-nm HC-PBGF

An additional application of this HC-PBGF-filling method is found in the area of high harmonic generation. The ability to introduce gas directly into the fiber core would eliminate any undesired nonlinear and absorption effects while coupling into and out of the fiber (see chapter 5). For the studies described in the next chapter this requires drilling through a HC-800-02 hollow core fiber designed with band-gap transmission centered around 830 nm. In transferring

this microchannel drilling process described here to this fiber some issues are encountered leading to modifications in our experimental setup.

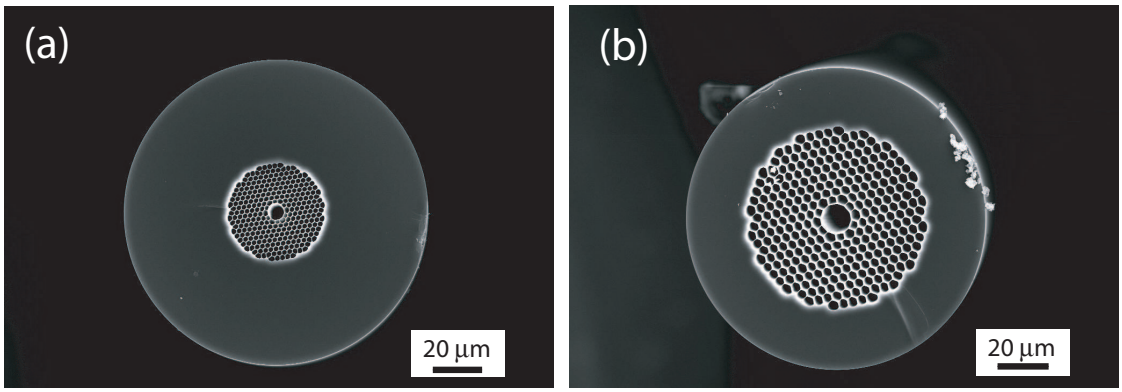

Figure 4.3: Scanning electron micrograph images of (a) HC-800-02 and (b) HC-1550-02 hollow-core fiber

As required by the guidance mechanism of these fibers the microstructure region in our original HC-1550-02 shows a much larger set of core-surrounding capillaries and has a pitch spacing of 3.8 μm while the pitch for the HC-800-02 fiber is only 2.2 μm, Figure 4.3. In describing fluid flow in a long cylindrical tube, Poiseuille's equation gives the flux Q to be fourth-order dependent upon the radius a of the tube [5]

$$Q = \frac{\pi G a^4}{8\mu}, \tag{4.1}$$

where G is the pressure gradient and μ is the dynamic viscosity. For a comparable pressure this results in nearly an order of magnitude drop in the index-matching fluid flux through the HC-800-02 fiber. In addition, the surrounding glass of the HC-800-02 fiber is 15 μm thicker than the HC-1550-02 producing 50% more glass to machine through. These changes in the fiber structure com-

bine to frustrate drilling as material buildup in the capillaries prevent debris removal. To eliminate this issue in drilling through the HC-800-02 fiber the index-matching fluid is replaced by the lower-viscosity methanol flowing through the core and microstructure region for efficient debris removal.

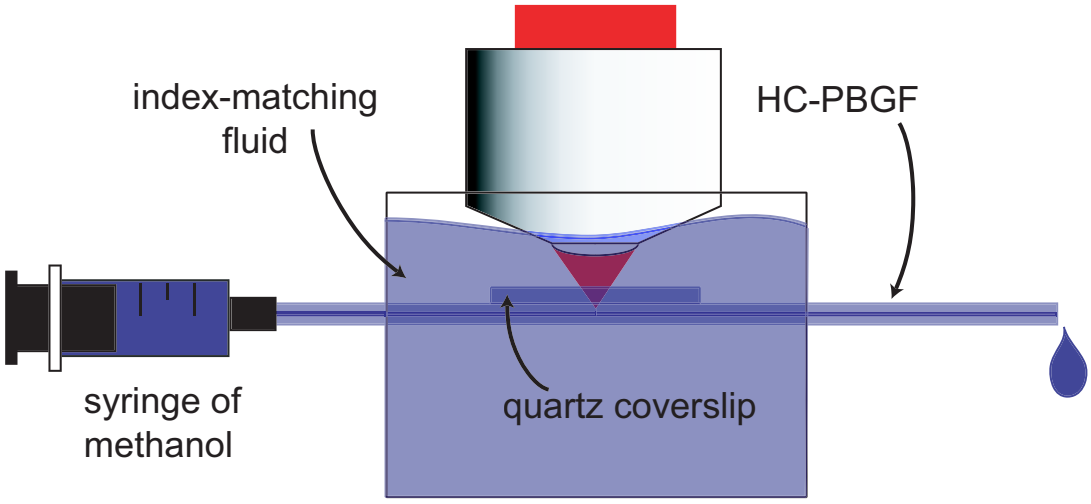

Figure 4.4: Modified experimental setup for microchannel drilling in HC-800-02 fiber using a quartz coverslip to suppress bubble formation on the fiber surface.

For microchannel production in a HC-800-02 fiber we use a regeneratively amplified laser system (Coherent Rega) operating at 250-kHz repetition rate, centered at 800 nm and producing 90-fs pulses. Drilling is done at 160-nJ pulse energies and the fiber translated at a rate of 10 μm/s. With methanol being injected through the fiber to remove debris, microchannel formation was still impeded by bubble formation at the surface. Observed by previous investigations [6] this optical breakdown in the index-matching fluid prevents drilling as the focus nears the glass-fluid surface causing a microchannel that stops several micrometers from the edge of the fiber. Although etching with hydrofluoric acid has been utilized to remove the remaining glass at the surface [6] this is

not a viable option for HC-PBGFs with the delicate microstructure region that would be susceptible to etching. As an alternative, we eliminate bubble formation by increasing the distance between the femtosecond laser focus and the glass-fluid surface by positioning a quartz coverslip (see Figure 4.4) on top of the fiber. Micromachining can then proceed and a 2-3 μm microchannel free of debris formed from the surface to the core by drilling into the backside of this coverslip. This method requires no complicated post-processing and has potential for rapid production of sub-micrometer channels.

4.3 Microchannel Effect on Optical Transmission

In order to be a viable means of filling and evacuating the HC-PBGF for gas-cell applications, the microchannel must not substantially reduce the optical transmission of the fiber. To measure the loss produced by drilling through the side of the fiber, a cutback method is employed. Six evenly spaced holes are drilled over a 2-mm section of a 33-cm length of HC-PBGF (Crystal Fibre, HC-1550-02). Fusion splicing the HC-PBGF to a fiber-coupled broadband source allows for a consistent measure of throughput without altering the input coupling. Spectral transmission measurements are then taken before and after the laser-drilled region is cutback (Fig. 4.5). The measured loss due to the drilled region of the fiber is found to be approximately 2.1 dB from 1500-1550 nm. Since the intrinsic loss of the fiber at these wavelengths is negligible (¡ 0.1 dB/m), this yields an estimated loss of 0.35 dB for a single drilled microchannel. We have no explanation, at this time, for the spectral dependence of the loss due to the microchannels.

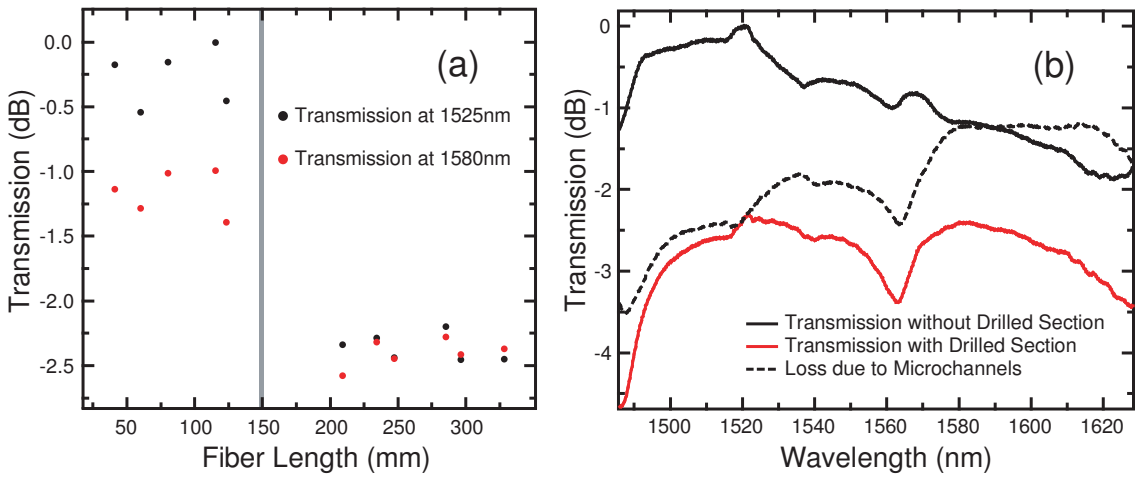

Figure 4.5: (a) Cutback measurements taken along the length of the fiber. The drilled section is located at 150 mm (gray). (b) Averaged HC-1550-02 spectral transmission with (red) and without (black) laser-drilled section, both spectra are normalized to peak transmission before drilling. Subtracting these two plots gives the loss due to the drilled section (dashed line).

4.4 Variable-Pressure Acetylene Fiber Cell

To create the hollow-core fiber cell, a microchannel is drilled from the core to the surface of a HC-PBGF (Crystal Fibre, HC-1550-01), and the index-matching fluid is removed from the fiber as described above. Each end of the HC-PBGF is then fusion spliced to step-index fiber using the parameters recently described in the literature [7]. Holding the drilled section of the fiber in a small vacuum chamber allows for a long, variable-pressure interaction length, while readily connecting to fiber-coupled devices (see Fig. 4.6). After evacuating the system for 30 minutes to a pressure of several mTorr, it is then filled at two different backing pressures. Several minutes following the introduction of acetylene a steady-state in pressure is achieved and transmitted spectra are measured. As shown in the spectra normalized to the band-gap transmission of the evacuated fiber,

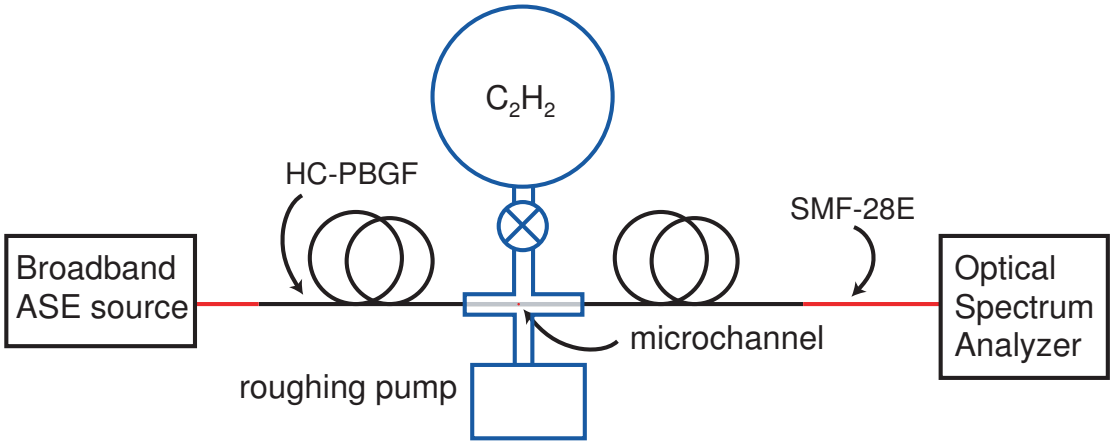

Figure 4.6: Experimental setup for acetylene filling. The laser-drilled hole is held inside a vacuum cell, which is evacuated with a roughing pump. The fiber jacket to vacuum chamber is sealed with a low vapor-pressure epoxy resin.

increased absorption occurs with increased pressure (see Fig. 4.7). These spectra are consistent with similar measurements from previous HC-PBGF acetylene gas cell work [1]. The measured loss through the system is found to be 5.6 dB, which is due primarily to the splice loss between the HC-PBGF and the step-index fiber.

In summary, we have used femtosecond pulses to drill microchannels into the side of a hollow-core photonic band-gap fiber. As a demonstration of its capability as a fiber cell, acetylene spectra were measured at two different backing pressures. We also measured the loss due to a single drilled microchannel to be approximately 0.35 dB. Still to be investigated are possible high pressure applications for this all-fiber variable-pressure gas cell, where a compact, tunable source of nonlinearity is required. These include tunable gain in a Raman scattering source or tunable pulse compression following a fiber laser. At low pressures this system has the potential for a myriad of spectroscopic and gas

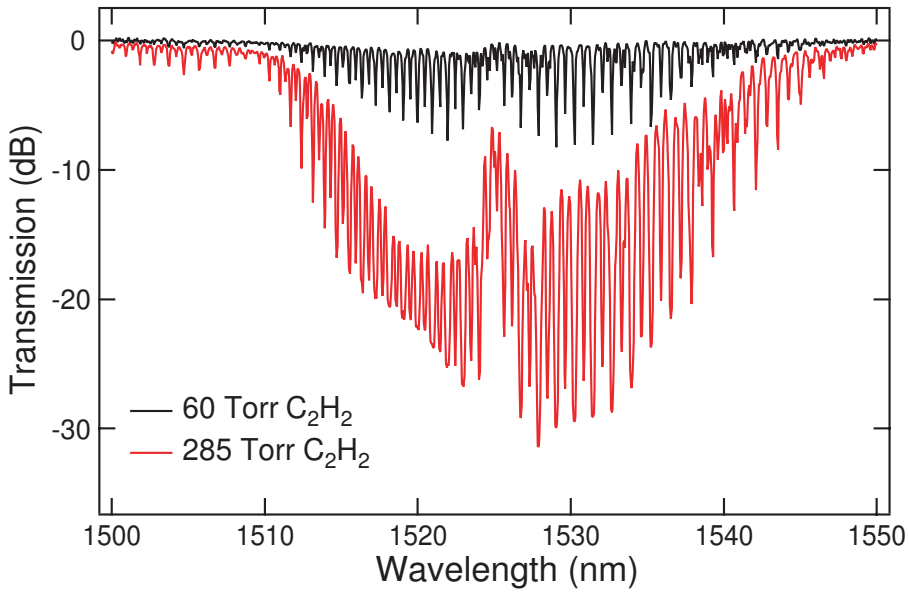

Figure 4.7: Vibrational-rotational spectra of acetylene filled HC-PBGF. These spectra are taken by measuring transmission through a 72-cm length of hollow core fiber and are normalized to the fiber band-gap transmission.

sensing applications.

Shortly following publication of this work an alternative approach was demonstrated for drilling through the side wall of a hollow-core fiber with femtosecond-laser pulses [8].

REFERENCES

[1] F. Benabid, F. Couny, J. C. Knight, T. A. Birks, and P. St. J. Russell, *Nature* **434**, 488-491 (2005).

[2] P. S. Light, F. Couny, and F. Benabid, *Opt. Lett.* **31**, 2538-2540 (2006).

[3] S. Nolte, C. Momma, G. Kamlage, A. Ostendorf, C. Fallnich, F. von Alvensleben, and H. Welling, *Appl. Phys. A* **68**, 563-567 (1999).

[4] Y. Lai, K. Zhou, L. Zhang, and I. Bennion, *Opt. Lett.* **31**, 2559-2561 (2006).

[5] G. K. Batchelor, *An Introduction to Fluid Dynamics* (Cambridge University Press, 1967).

[6] R. An, J. D. Uram, E. C. Yusko, K. Ke, M. Mayer, and A. J. Hunt, *Opt. Lett.* **33**, 1153-1155 (2008)

[7] R. Thapa, K. Knabe, K. L. Corwin, and B. R. Washburn, *Opt. Express* **14**, 9576-9583 (2006).

[8] A. van Brakel, C. Grivas, M. N. Petrovich, and D. J. Richardson, *Opt. Express* **15**, 8731-8736 (2007)

CHAPTER 5

HIGH-HARMONIC GENERATION IN HOLLOW-CORE PHOTONIC BAND-GAP FIBER

In this chapter we present experimental studies directed toward the demonstration of high-harmonic generation in a hollow-core photonic band-gap fiber (HC-PBGF). Although high harmonics were not observed, a number of experimental steps were taken toward this goal. This along with a proposed mechanism for quasi-phase matching high harmonic generation in HC-PBGFs will be discussed in this chapter.

High harmonic generation is an intense field interaction with gas that generates odd harmonics of the fundamental driving laser [1]. Hollow-core photonic band-gap fibers have emerged as a novel approach for studying laser-gas interactions in a tightly-confined geometry [2]. With single-mode guidance and mode-field diameters less than 5 μm for near-infrared light, pulse intensities on the order of 10^{14} W/cm^2 can be transmitted over thousands of Rayleigh lengths. Here we attempt to utilize these properties in the area of high harmonic generation in a gas-filled photonic band-gap fiber core.

5.1 Experimental Methods

In this experiment the driving fundamental for the high harmonics is produced by a regeneratively amplified Ti-Sapphire laser producing 50-fs pulses at a 1-kHz repetition rate centered at 810 nm. As shown in the experimental setup (Figure 5.1), the HC-PBGF (Crystal Fibre, HC-800-02) is held inside a chamber evacuated with a turbo pump to a pressure of 10^{-5} torr. Following the same

method described in Chapter 3 the amplified laser is spatially filtered and mode matched to the HC-PBGF using an aspheric objective lens. To introduce xenon, the fiber is mounted in a microfluidic tee (Labsmith, C360-203), and gas continuously flows through a microchannel drilled into the side of the fiber using the technique described in section 4.2 of this dissertation. Only a 15-mm length of fiber is used to avoid absorption effects from the gas. Even with a short length of fiber being used, we still have an interaction length 500 times the confocal parameter that these focusing conditions would create in a gas cell or jet.

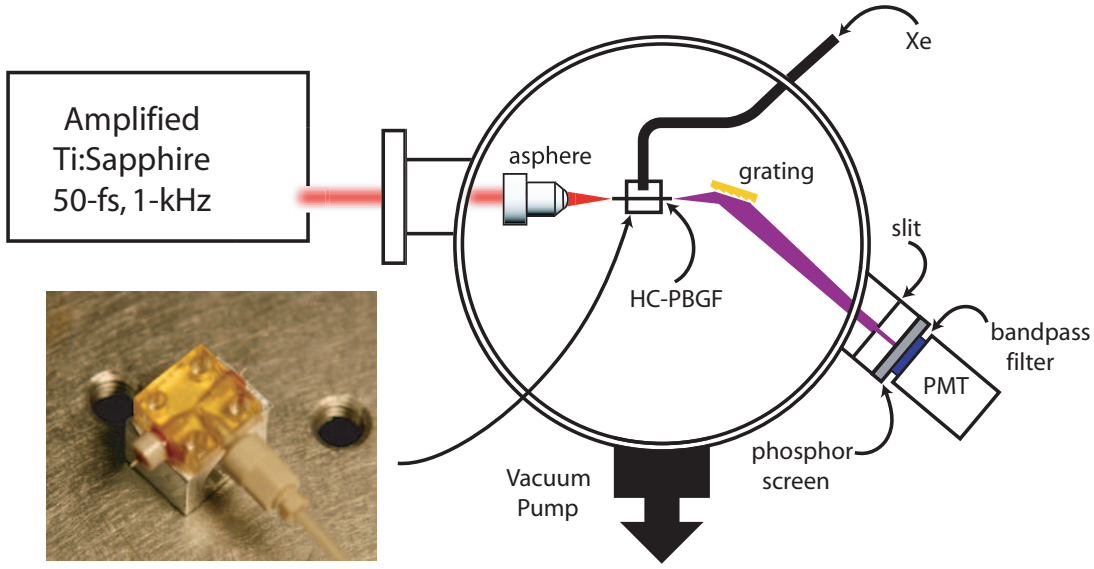

Figure 5.1: Experimental setup for generating and observing high harmonic generation.

Coupling into the fiber is controlled by mounting the fiber on a three-axis piezo-controlled stage inside of the chamber. When the system is evacuated, this coupling is disturbed and optimization is re-established using a large-area silicon photodiode (Hamamatsu, S1227-1010BR) that swings in and out of the path of the fiber output. Once coupling into the fundamental core mode is achieved,

this photodiode is removed from the beam path and the fiber output falls onto an aberration-corrected concave grating (Hitachi, 001-0639) 10 cm from the fiber output. This diffraction grating, designed to operate in the extreme ultraviolet, is rotated to direct individual harmonics toward a 1-mm slit positioned 20 cm from the grating for detection, Figure 5.1.

5.2 Extreme Ultraviolet Detection

Radiation produced by high harmonic generation extends into the vacuum (200-10 nm) and extreme (121-10 nm) ultraviolet regime. As these short wavelengths are quickly absorbed by air, they require an evacuated chamber to propagate. Detection is problematic since the conversion efficiency is very low and the most sensitive photon detection methods (e.g. avalanche photodiode, photomultiplier tubes) have been developed for visible light. To circumvent this issue we use a phosphor screen of sodium salicylate that is excited by the incident harmonic radiation and emits fluorescence between 380-440 nm [3]. This method is commonly used for detecting vacuum ultraviolet radiation since the quantum efficiency is relatively constant for excitation from 10-350 nm [4, 5, 6, 7, 8]. A sodium salicylate coated window is then mounted directly behind the slit and fluorescence is detected with a bialkali photomultiplier tube (Hamamatsu, H10425) with peak sensitivity at 420 nm. To eliminate any scattered fundamental an optical bandpass filter (Chroma, D405/90x) centered at 405 nm is inserted between the phosphor window and photomultiplier tube.

A preliminary demonstration with a jet of xenon calibrates our detection system. Using a 15-cm lens, 50-μJ pulse energies are focused into a continuous

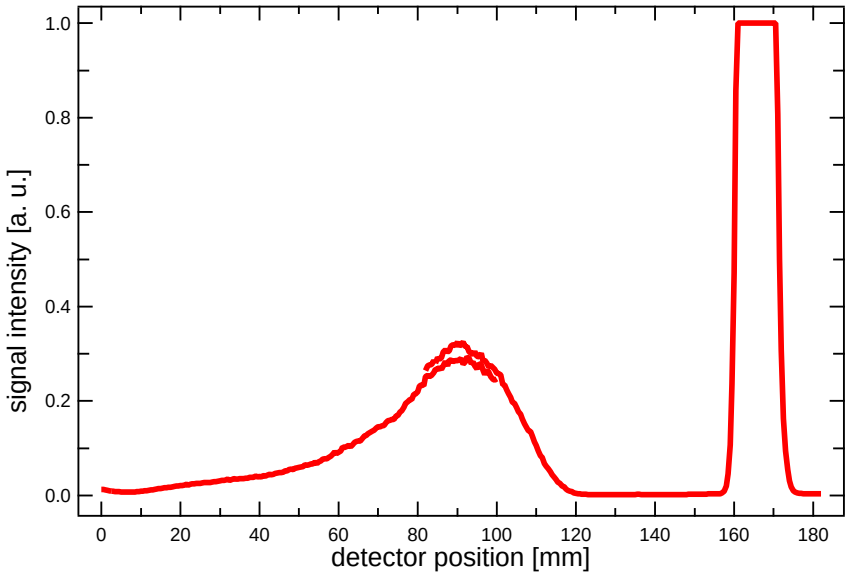

Figure 5.2: Signal from the photomultiplier tube when focusing 50-μJ pulses into a continuous stream of xenon. The large signal on the right is due to zero-order reflection from the grating. This trace was taken with two scans of the linear stage.

stream of xenon gas, producing a peak intensity of $\sim 5 \times 10^{13}$ W/cm^2. This gas jet is produced at the end of an open capillary tube with an inner diameter of 250-μm. Backing pressure for this experiment was 20-30 psi. In an unevacuated chamber, we were able to observe a substantial signal corresponding to the third harmonic with a stationary grating and scanning this detector with a linear stage (Figure 5.2). Any higher harmonics would be quickly absorbed by the surrounding air (see Figure 5.3). When moving to an evacuated chamber this third harmonic generation signal is not found. This is likely due to the large evacuation rate of the turbo pump preventing formation of an adequate xenon density to observe harmonic generation.

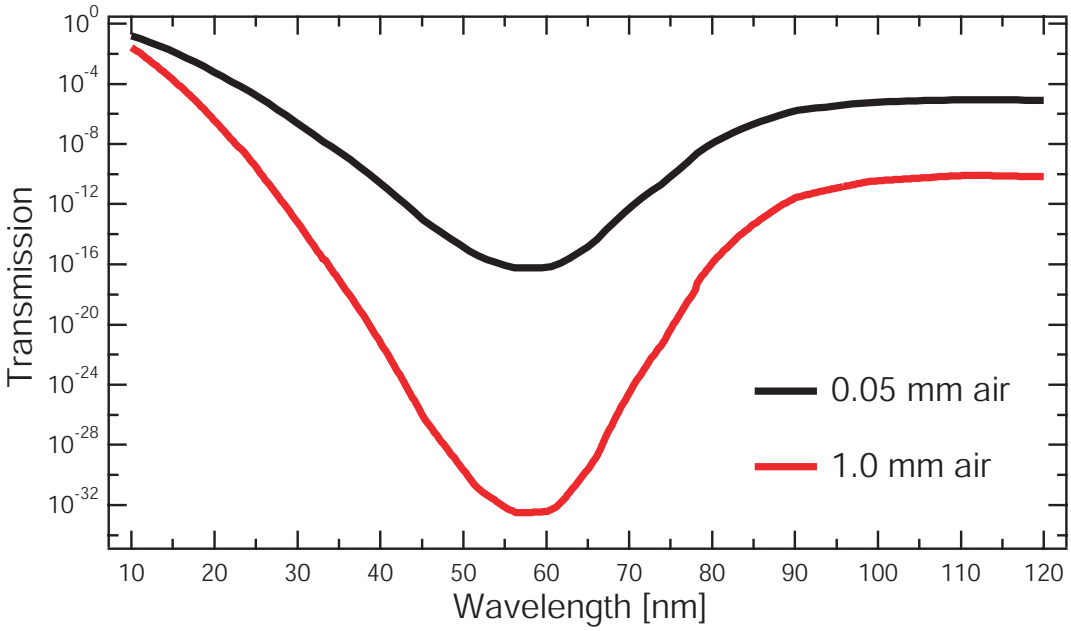

Figure 5.3: Transmission of extreme ultraviolet radiation through air at atmospheric pressure. Data from reference [9].

5.3 Phase Matching High Harmonic Generation in HC-PBGF

Previous theoretical work has studied the potential for phase-matching of high harmonic generation in HC-PBGF [10]. Although the band-gap guidance of the HC-800-02 fiber used in this experiment is limited to 780-880 nm, for sufficiently high harmonics guidance can be achieved by total internal reflection. As shown in Figure 5.4, the index of refraction of silica glass drops to less than that of the gas-filled core (~1.0) allowing for this extreme ultraviolet radiation to be guided along with the fundamental. This separate guidance mechanism allows for phase-matching of the fundamental and selective high harmonics by matching the effective refractive indexes. Since the waveguide contribution is constant, pressure-tuning the gas should allow for adjustment of these values. More

recent analysis has shown broadband phase-matching through soliton propagation effects [11].

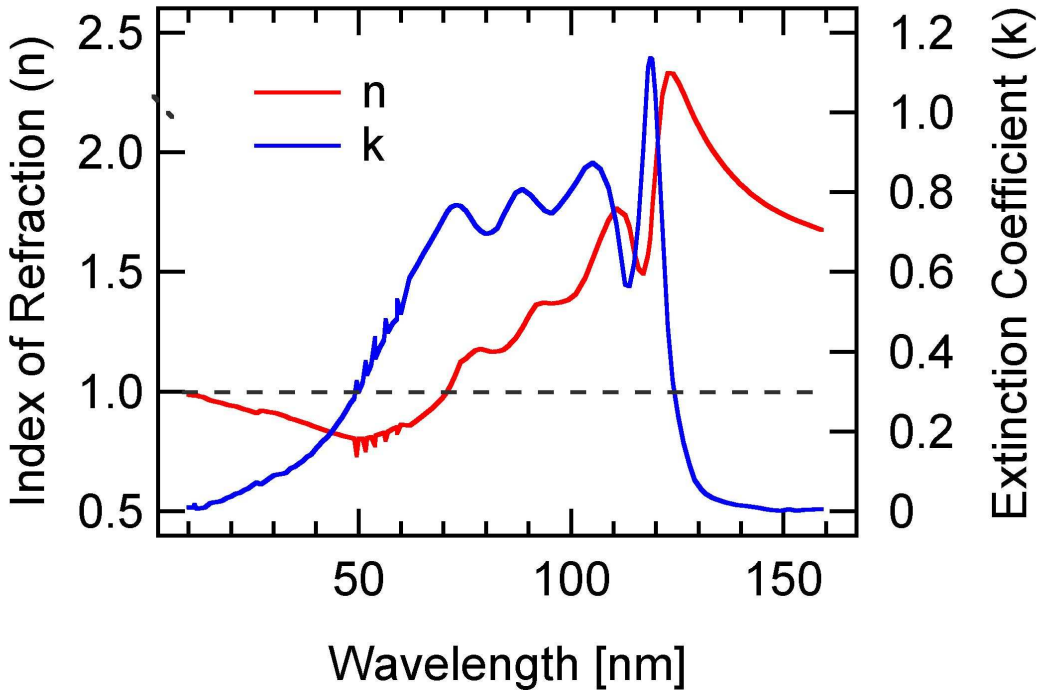

Figure 5.4: Plot of the index of refraction and extinction coefficient for silica glass in the extreme ultraviolet regime.

Another method for enhancing the efficiency of this process is quasi-phase matching. First demonstrated for high harmonic generation in glass capillaries [13], quasi-phase matching involves modifying the nonlinearity on a period equal to the inverse of the phase-mismatch of the harmonic process [12]. This can be understood by looking at the solution for a qth order harmonic field amplitude,

$$E_q(L) = iE_1^q \int_0^L \gamma_q(z) e^{i\Delta kz} dz, \tag{5.1}$$

where E_1 is the amplitude of the fundamental, L is the length of the nonlinear medium, $\triangle k$ is the amplitude of the wave-vector mismatch given by,

$$\triangle\, k = \frac{q\omega_1}{c}(n_1 - n_q), \tag{5.2}$$

where n_1 and n_q are the refractive indices at the fundamental and harmonic frequencies respectively, and $\gamma_q(z)$ is the nonlinear parameter which is dependent on the qth-order nonlinearity coefficient $\chi^{(q)}(z)$ and can be expressed as,

$$\gamma_q(z) = \frac{2\pi q\omega_1}{n_q c}\chi^{(q)}(z). \tag{5.3}$$

If the nonlinear parameter γ_q contains a Fourier component $e^{-i\triangle kz}$, then this component will be effectively phase matched allowing for efficient generation of the harmonic. For periodically-poled materials, the sign of $\chi^{(2)}$ and thus γ_2 can be periodically switched, which means that phase matching can occur with a nonlinear coefficient that is only a factor of two less than the bulk value. Alternatively, for nonlinear interactions where the sign cannot be changed but the magnitude of γ_q can be modulated such that

$$\gamma_q(z) = \gamma_q^{dc} + \frac{1}{2}\gamma_q^{mod}(e^{i\triangle kz} + e^{-i\triangle kz}). \tag{5.4}$$

For the case of a hollow waveguide this perturbation can be achieved by periodically modulating the diameter of the core and thus the effective nonlinearity of the waveguide. The desired modulation period for harmonic generation can be expressed in terms of the phase-mismatch via the relation

$$\Lambda = \frac{2\pi}{|\triangle k|} = \frac{\lambda_1}{q\,|\triangle n_q^{gas} + \triangle n_q^{wg}|}, \tag{5.5}$$

when the waveguide contribution to the index mismatch dominates, the period can be approximated by,

$$\Lambda \approx \frac{\lambda_1}{q \triangle n_q^{wg}} \approx \frac{8\pi^2 a^2}{q\lambda_1 u_{11}^2}, \tag{5.6}$$

where a is the radius of the waveguide and u_{11} is the first zero for the zero-order Bessel function from the waveguide solution [14]. For the HC-PBGF used in this work, with a mode-field diameter of 5 μm, this would correspond to modulation period of 6.2-3.4 μm for high harmonics in the range of 50-25 nm.

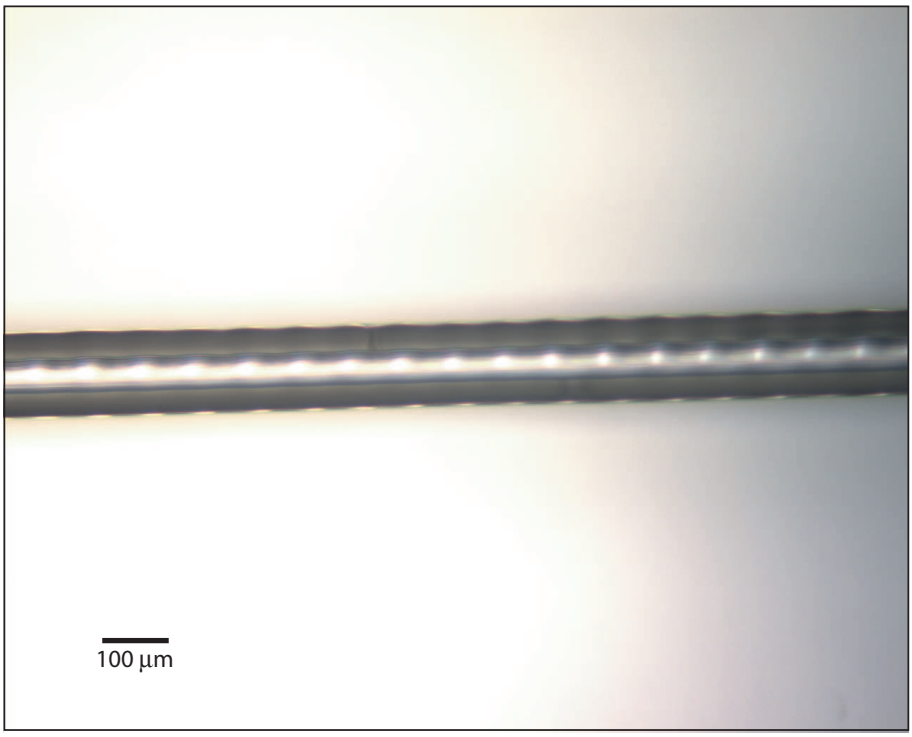

Figure 5.5: Optical microscope image of HC-PBGF periodically tapered by selective heating and pulling of the fiber with a carbon-dioxide laser.

In a demonstration of this modulation, a carbon dioxide laser was used to periodically taper a HC-PBGF. As can be seen from the image (Figure 5.5), delocalized heating of the fiber limited the achievable period of modulation to ~80 μm. However, using the ultrafast-laser machining method previously demonstrated in chapter 4 of this dissertation it should be possible to produce a periodic structure of several micrometers in a HC-PBGF. An alternative procedure for quasi-phase matching high harmonic generation in HC-PBGF has been proposed in the literature using a counter-propagating laser [15].

In summary, we have utilized results from previous chapters in an effort to experimentally observe high harmonic generation in a HC-PBGF. Though extreme ultraviolet radiation is yet to be detected, some issues related to this work have been overcome and at this point we assume the reduced gas density within the fiber core to be the limiting factor. We have also outlined a possible method for quasi-phase matching this process inside of a hollow-core fiber by periodic modulation using ultrafast-laser micromachining.

REFERENCES

[1] P. B. Corkum, *Phys. Rev. Lett.* **71** 1994 (1993).

[2] R. F. Cregan, B. J. Mangan, J. C. Knight, T. A. Birks, P. St. J. Russell, P. J. Roberts, and D. A. Allan, *Science* **285**, 1537-1539 (1999).

[3] D. H. Thurnau, *J. Opt. Soc. Am.* **46**, 346-346 (1956).

[4] F. S. Johnson, K. Watanabe, and R. Tousey, *J. Opt. Soc. Am.* **41**, 702 (1951).

[5] K. Watanabe and E. C. Y. Inn, *J. Opt. Soc. Am.* **43**, 32 (1953).

[6] J. A. R. Samson, *J. Opt. Soc. Am.* **54**, 6 (1964).

[7] R. A. Knapp and A. M. Smith, *Appl. Opt.* **3**, 637 (1964).

[8] J. A. R. Samson and G. N. Haddad, *J. Opt. Soc. Am.* **64**, 1346 (1974).

[9] B.L. Henke, E.M. Gullikson, and J.C. Davis, *Atomic Data and Nuclear Data Tables* Vol. **54** (no.2), 181-342 (July 1993).

[10] E. E. Serebryannikov, D. von der Linde, and A. M. Zheltikov, *Phys. Rev. E.* **70**, 066619 (2004).

[11] E. E. Serebryannikov, D. von der Linde, and A. M. Zheltikov, *Opt. Lett.* **33**, 977-979 (2008).

[12] M.M. Fejer, G. A. Magel, D. H. Jundt, and R. L. Byer, *IEEE J. Quantum Electron.* **28**, 2631 (1992).

[13] E. A. Gibson, A. Paul, N. Wagner, R. Tobey, D. Gaudiosi, S. Backus, I. P. Christov, A. Aquila, E. M. Gullikson, D. T. Attwood, M. M. Murnane, and H. C. Kapteyn, *Science* **302**, 9598 (2003).

[14] A. W. Snyder and J. D. Love, *Optical Waveguide Theory* (Kluwer Academic Publishers, 1983).

[15] H. Ren, A. Nazarkin, J. Nold, and Philip S. Russell, *Opt. Express* **16**, 17052-17059 (2008).

CHAPTER 6

CONCLUSION AND FUTURE WORK

The primary aim of this dissertation has been the study of intense laser propagation in hollow-core photonic band-gap fibers (HC-PBGFs). Though the goal of observing high harmonics generation in a gas-filled HC-PBGF has not been achieved a number of important barriers to this experimental success have been removed. The experiments in this thesis present steps toward that goal and open up new areas for investigation, this chapter will summarize these results and discuss future work.

Toward the goal of high harmonic generation in a gas-filled HC-PBGF this dissertation presents a number of advancements. To begin, the studies of low-loss coupling into these fibers dramatically enhanced the peak intensity transmitted through these fibers [1]. By careful mode-matching we demonstrated 98% coupling and 1.6×10^{14} W/cm^2 delivered peak intensity, well into the regime for producing high harmonics. Next, using tightly focused femtosecond-laser pulses we were able to drill through the side of a HC-PBGF for direct filling of the fiber core [2]. Along with producing a variable-pressure all-fiber gas cell, we also created an ideal means of introducing gas into the fiber for high harmonic generation. With gas introduced through the side, the input and output of the fiber can sit in an evacuated cell which avoids any nonlinear interaction as the beam is coupled into the fiber and eliminates absorption effects at the output. This work is complemented by the high-peak transmission studies of Chapter 3, allowing for intense laser-gas interaction in the fiber core while still maintaining our stringent coupling requirements. As discussed in Chapter 5 the generated vacuum ultraviolet light is quickly absorbed by air and also by the

noble gas (see Figure 6.1). Recent work from a large, collaborative effort has reported observation of harmonics as high as 13th in a xenon-filled Kagome-type photonic crystal fiber [3]. The experimental setup in this work did have xenon present in a front cell leaving ambiguity as to the were the harmonics are being generated. Finally, the work presented in Chapter 5 details the experimental effort that has been done to combine all of these steps including optimizing coupling inside the evacuated chamber, the introduction of gas into the fiber and the complicated detection scheme required for these harmonic wavelengths.

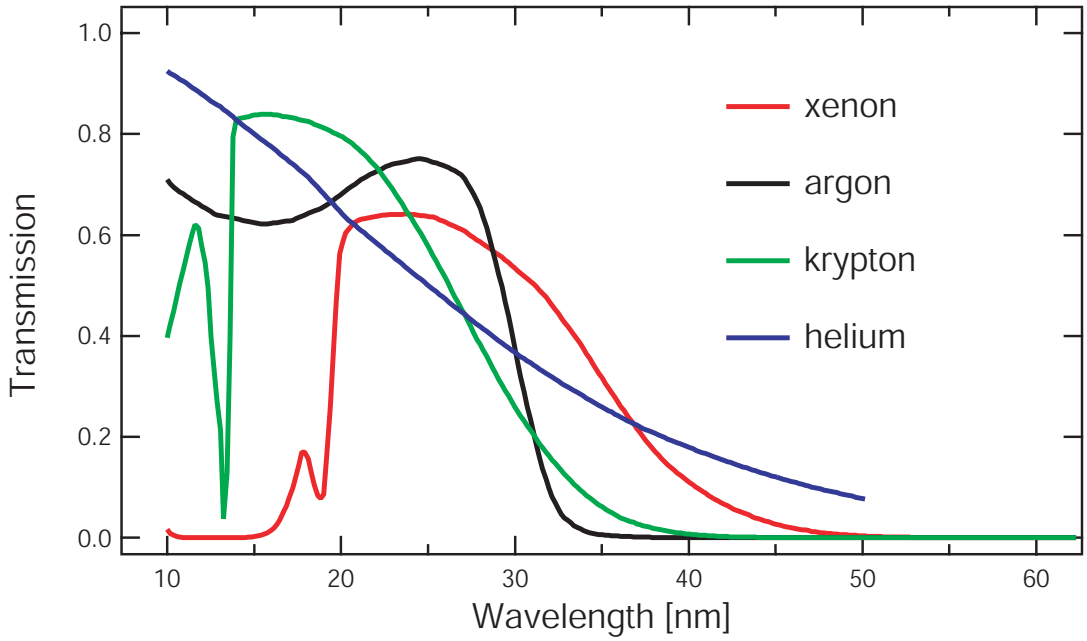

Figure 6.1: Transmission of extreme ultraviolet radiation through 1 cm of various noble gases used for high harmonic generation. Data taken at 10 torr pressures from reference [4].

Although the separate guiding mechanisms for the fundamental and generated harmonics should allow for pressure-tuned phase matching [5], quasi-phase matching is also an option for enhancing conversion. As in previous

work, that demonstrated quasi-phase matching by periodically modulating a hollow capillary [6], the ability to periodically perturb the fundamental mode in a HC-PBGF should produce a similar result. With the three-dimensional isolation that machining with femtosecond lasers allows for, it would be possible to remove material from the fiber core wall without disturbing the surrounding microstructure. This method would allow for quasi-phase matching inside a HC-PBGF without introducing losses into the fiber transmission.

By shrinking the period of this modulation, it should be possible to write a Bragg grating structure along the core wall of a HC-PBGF. In studying the silica-glass contribution to the nonlinearity of these fibers, we effectively measured the fraction of the fundamental mode that resides in the the glass wall of these fibers [7]. While this gives a theoretical limit for free-space coupling efficiency it also indicates a mechanism for periodic perturbation of the fiber mode. By drilling through the core wall with a femtosecond laser a large enough perturbation to the index of refraction should be created to cause a reflection from such a Bragg structure. According to the measurements presented in Chapter 2 two of this dissertation, approximately 0.1% of the fundamental mode resides in glass for a typical HC-PBGF operating at a center wavelength of 1550 nm. Removing material from the core wall as shown in Figure 6.2 would create an index of refraction change of $\sim 10^{-4}$-10^{-5} which is on the order of that found in commercial fiber Bragg gratings.

Using ultrafast-laser machining to write a fiber Bragg grating on a HC-PBGF would be an impressive demonstration of sub-micrometer fabrication inside a transparent structure. Such a grating would also be ideal for forming a low-loss cavity inside these fibers, opening up applications for unique studies of cavity-

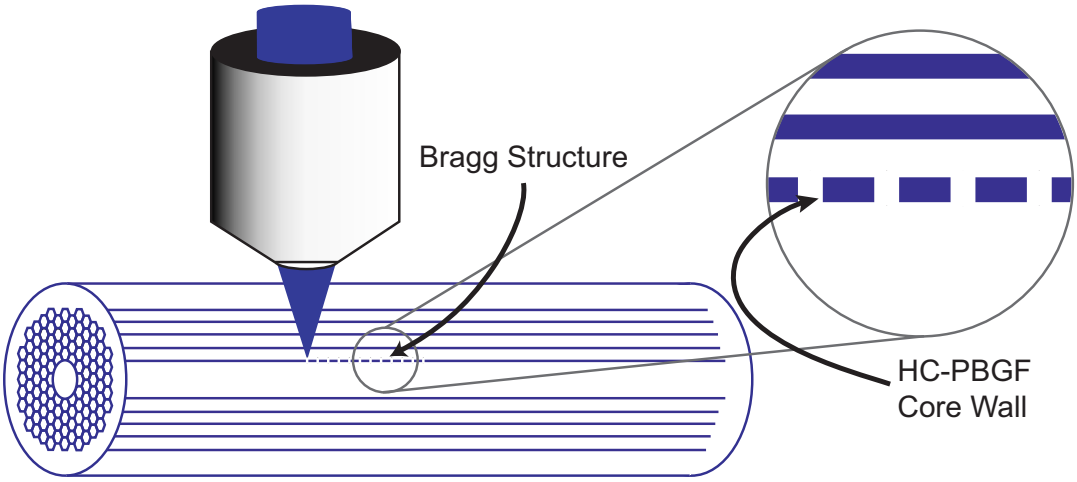

Figure 6.2: Proposed structure for writing a fiber Bragg grating in a HC-PBGF. A similar method could be used for quasi-phase matching high harmonic generation.

enhanced interactions. The point-by-point writing of a femtosecond-laser written grating would also allow for a chirped-Bragg grating to be written inside a fiber allowing for both stretching and compression in a single fiber making them an ideal component for high power fiber amplifier systems. The unique confinement and interaction lengths of HC-PBGFs have already led to a number of applications, through the work presented here we hope to extend the capabilities of these fibers and open up new areas for exploration.

REFERENCES

[1] A. A. Ishaaya, C. J. Hensley, B. Shim, S. Schrauth, K. W. Koch, and A. L. Gaeta, *in Preparation*.

[2] C. J. Hensley, D. H. Broaddus, C. B. Schaffer, and A. L. Gaeta, *Opt. Express* **15**, 6690-6695 (2007).

[3] C. R. Baer, O. H. Heckl, C. Krnkel, S. V. Marchese, F. Schapper, M. Holler, T. Sdmeyer, U. Keller, J. S. Robinson, J. W. Tisch, F. Couny, P. Light, F. Benabid, and P. S. Russell, *in Advanced Solid-State Photonics, OSA Technical Digest Series* (CD) (Optical Society of America, 2009), paper MF6.

[4] B.L. Henke, E.M. Gullikson, and J.C. Davis, *Atomic Data and Nuclear Data Tables* Vol. **54** (no.2), 181-342 (July 1993).

[5] E. E. Serebryannikov, D. von der Linde, and A. M. Zheltikov, *Phys. Rev. E.* **70**, 066619 (2004).

[6] E. A. Gibson, A. Paul, N. Wagner, R. Tobey, D. Gaudiosi, S. Backus, I. P. Christov, A. Aquila, E. M. Gullikson, D. T. Attwood, M. M. Murnane, and H. C. Kapteyn, *Science* **302**, 9598 (2003).

[7] C. J. Hensley, D. G. Ouzounov, A. L. Gaeta, N. Venkataraman, M. T. Gallagher, and K. W. Koch, *Opt. Express* **15**, 3507-3512 (2007).